

AD-A137 558

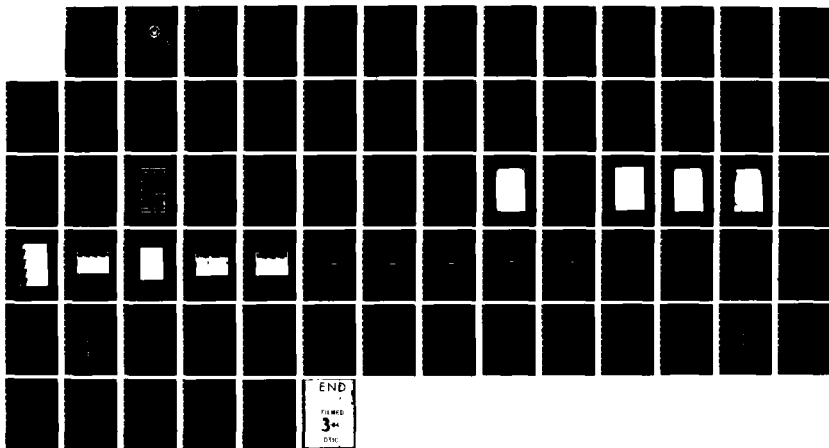
DETERMINATION OF BOUNDARY LAYER TRANSITION AND
SEPARATION ON DOUBLE CURVED (U) NAVAL POSTGRADUATE
SCHOOL MONTEREY CA A G MCGUIRE SEP 83

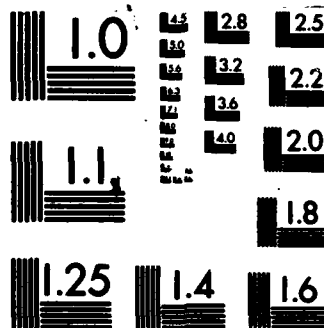
1/1

UNCLASSIFIED

F/G 28/4

NL





MICROCOPY RESOLUTION TEST CHART
NATIONAL BUREAU OF STANDARDS-1963-A

2

NAVAL POSTGRADUATE SCHOOL

Monterey, California



AD A137550

THESIS

DTIC
ELECTED
S FEB 6 1984
A

DETERMINATION OF BOUNDARY LAYER TRANSITION
AND SEPARATION ON DOUBLE CIRCULAR ARC
COMPRESSOR BLADES IN A LARGE SUBSONIC CASCADE

by

Alan G. McGuire

September 1983

Thesis Advisor:

Raymond P. Shreeve

Approved for public release; distribution unlimited.

DTIC FILE COPY

84 02 6 111

UNCLASSIFIED

SECURITY CLASSIFICATION OF THIS PAGE (When Data Entered)

REPORT DOCUMENTATION PAGE		READ INSTRUCTIONS BEFORE COMPLETING FORM
1. REPORT NUMBER	2. GOVT ACCESSION NO.	3. RECIPIENT'S CATALOG NUMBER
4. TITLE (and Subtitle) Determination of Boundary Layer Transition and Separation on Double Arc Compressor Blades in a Large Subsonic Cascade		5. TYPE OF REPORT & PERIOD COVERED Master's Thesis September 1983
7. AUTHOR(s) Alan G. McGuire		6. PERFORMING ORG. REPORT NUMBER
8. PERFORMING ORGANIZATION NAME AND ADDRESS Naval Postgraduate School Monterey, California 93943		9. CONTRACT OR GRANT NUMBER(s)
11. CONTROLLING OFFICE NAME AND ADDRESS Naval Postgraduate School Monterey, California 93943		10. PROGRAM ELEMENT, PROJECT, TASK AREA & WORK UNIT NUMBERS
14. MONITORING AGENCY NAME & ADDRESS (if different from Controlling Office)		12. REPORT DATE September 1983
		13. NUMBER OF PAGES 72
		15. SECURITY CLASS. (of this report) UNCLASSIFIED
		15a. DECLASSIFICATION/DOWNGRADING SCHEDULE
16. DISTRIBUTION STATEMENT (of this Report) Approved for public release; distribution unlimited.		
17. DISTRIBUTION STATEMENT (of the abstract entered in Block 20, if different from Report)		
18. SUPPLEMENTARY NOTES		
19. KEY WORDS (Continue on reverse side if necessary and identify by block number) Cascade DCA Blading Flow Visualization		
20. ABSTRACT (Continue on reverse side if necessary and identify by block number) The china clay technique for flow visualization was used to determine the surface flow on a double circular arc (DCA) compressor blade in a large rectilinear subsonic cascade wind tunnel. A calibration experiment using a large flat plate model is also reported which allowed the drying patterns on the DCA blading to be interpreted. Natural transition occurred on the flat plate at a Reynolds Number based on transition		

DD FORM 1 JAN 73 1473

EDITION OF 1 NOV 68 IS OBSOLETE

S/N 0102-LF-014-6601

1

UNCLASSIFIED

SECURITY CLASSIFICATION OF THIS PAGE (When Data Entered)

UNCLASSIFIED

SECURITY CLASSIFICATION OF THIS PAGE (When Data Entered)

location of 0.8×10^6 , and on the suction surface of the DCA blading at significant negative incidence angles at a Reynolds Number based on transition location of approximately 0.5×10^6 . At incidence angles larger than -3° , the DCA blade showed a leading edge separation bubble with turbulent reattachment.



A-1

S-N 0102-LF-014-6601

UNCLASSIFIED

SECURITY CLASSIFICATION OF THIS PAGE (When Data Entered)

Approved for public release; distribution unlimited.

Determination of Boundary Layer Transition
and Separation on Double Circular Arc Compressor
Blades in a Large Subsonic Cascade

by

Alan G. McGuire
B.S.A.E., California Polytechnic State University, 1972

Submitted in partial fulfillment of the
requirements for the degree of

MASTER OF SCIENCE IN AERONAUTICAL ENGINEERING

from the

NAVAL POSTGRADUATE SCHOOL
September 1983

Author:

Alan G. McGuire

Approved by:

Raymond P. Haseene

Thesis Advisor

Donald R. Lyster

Chairman, Department of Aeronautics

James

Dean of Science and Engineering

ABSTRACT


➤ The china clay technique for flow visualization was used to determine the surface flow on a double circular arc (DCA) compressor blade in a large rectilinear subsonic cascade wind tunnel. A calibration experiment using a large flat plate model is also reported which allowed the drying patterns on the DCA blading to be interpreted. Natural transition occurred on the flat plate at a Reynolds Number based on transition location of 0.8×10^6 ^(million) and on the suction surface of the DCA blading at significant negative incidence angles at a Reynolds Number based on transition location of approximately 0.5×10^6 ^{million}. At incidence angles larger than $-3 \frac{deg}{1}$ ^{deg}, the DCA blade showed a leading edge separation bubble with turbulent reattachment. 

TABLE OF CONTENTS

I.	INTRODUCTION	11
II.	TEST FACILITIES AND INSTRUMENTATION	13
	A. RECTILINEAR CASCADE	13
	B. INSTRUMENTATION	13
	C. CHINA CLAY TECHNIQUE	14
	D. TEST MODELS	16
	E. TEST PROCEDURE	17
III.	TEST PROGRAM AND RESULTS	18
	A. OUTLINE OF TESTS	18
	B. TEST PROGRAM	18
IV.	DISCUSSION	21
	A. FLAT PLATE EXPERIMENTS	21
	B. DCA BLADE EXPERIMENTS	23
V.	CONCLUSIONS	25
	TABLES	26
	FIGURES.	28
	APPENDIX A: PLENUM MODIFICATION	51
	LIST OF REFERENCES	71
	INITIAL DISTRIBUTION LIST	72

LIST OF TABLES

I.	NOMINAL FLOW VELOCITIES AND TEST REYNOLDS NUMBERS	26
II.	DCA BLADE CASCADE CONFIGURATION	27

LIST OF FIGURES

1.	CASCADE WIND TUNNEL TEST FACILITY	28
2.	CASCADE TEST SECTION SCHEMATIC	29
3.	DCA BLADE PROFILE	30
4.	FLAT PLATE PROFILE	31
5.	FEATURES OF BOUNDARY LAYER FLOW ON FLAT PLATE AT 0° INCIDENCE	32
6.	RELATIVE VALUES OF SURFACE HEAT TRANSFER RATES UNDER DIFFERENT FLOW CONDITIONS	33
7.	DRYING PATTERNS ON A FLAT PLATE WITH A SHARP LEADING EDGE ($i = -0.5^{\circ}$)	34
8.	TRANSITION LOCATION VS. REYNOLDS NUMBER FOR A FLAT PLATE	35
9a.	SURFACE FLOW PATTERN AT -4° INCIDENCE ON A FLAT PLATE WITH ROUNDED LEADING EDGE	36
9b.	SURFACE FLOW PATTERN AT 0° INCIDENCE ON A FLAT PLATE WITH ROUNDED LEADING EDGE	37
9c.	SURFACE FLOW PATTERN AT 4° INCIDENCE ON A FLAT PLATE WITH ROUNDED LEADING EDGE	38
10.	TRANSITION AND REATTACHMENT POINTS VS. INCIDENCE FOR FLAT PLATE WITH ROUNDED LEADING EDGE	39
11a.	SURFACE FLOW PATTERN ON DCA BLADE, $i = 8.8^{\circ}$	40
11b.	SURFACE FLOW PATTERN ON DCA BLADE, $i = 5.3^{\circ}$	41
11c.	SURFACE FLOW PATTERN ON DCA BLADE, $i = 2.1^{\circ}$	42
11d.	SURFACE FLOW PATTERN ON DCA BLADE, $i = -4.9^{\circ}$	43
11e.	SURFACE FLOW PATTERN ON DCA BLADE, $i = -9.2^{\circ}$	44
12a.	PRESSURE AND VELOCITY DISTRIBUTION ON THE DCA BLADE, $i = 8.8^{\circ}$	45

12b.	PRESSURE AND VELOCITY DISTRIBUTION ON THE DCA BLADE, $i = 5.3^0$	46
12c.	PRESSURE AND VELOCITY DISTRIBUTION ON THE DCA BLADE, $i = 2.1^0$	47
12d.	PRESSURE AND VELOCITY DISTRIBUTION ON THE DCA BLADE, $i = -4.9^0$	48
12e.	PRESSURE AND VELOCITY DISTRIBUTION ON THE DCA BLADE, $i = -9.1^0$	49
13.	DCA BLADE SUCTION SURFACE FLOW CHANGES WITH INCIDENCE ANGLE ($RE = 0.4 \times 10^6$)	50
A1.	RELATIVE VELOCITIES EXITING SOUND BAFFLES PRIOR TO MODIFICATION	54
A2.	NON-DIMENSIONAL PRESSURE VS. BLADE-TO-BLADE LOCATION WITH BAFFLES AND DIVERTER PLATE IN THE PLENUM	55
A3.	YAW ANGLE DISTRIBUTION WITH BAFFLES AND DIVERTER PLATE IN THE PLENUM	56
A4.	NON-DIMENSIONAL PRESSURE VS. BLADE-TO-BLADE LOCATION WITHOUT BAFFLES AND DIVERTER PLATE IN THE PLENUM	57
A5.	YAW ANGLE DISTRIBUTION WITHOUT BAFFLES AND DIVERTER PLATE IN THE PLENUM	58
A6.	DIFFUSING SCREEN ARRANGEMENT ON BLOWER EXIT	59
A7.	RELATIVE VELOCITIES EXITING SOUND BAFFLES WITH DIFFUSING SCREEN ARRANGEMENT ON THE BLOWER EXIT	60
A8a.	PLENUM TURNING VANES, SIDE VIEW	61
A8b.	PLENUM TURNING VANES, FRONT VIEW	62
A9.	NON-DIMENSIONAL PRESSURE VS. BLADE-TO-BLADE LOCATION WITH TURNING VANES IN THE PLENUM	63
A10.	YAW ANGLE DISTRIBUTION WITH TURNING VANES IN THE PLENUM	64
A11.	VORTEX FLOW AROUND ENDS OF THE TURNING VANES	65
A12.	ENCLOSED TURNING VANE ARRAY	66

A13.	NON-DIMENSIONAL PRESSURE VS. BLADE-TO-BLADE LOCATION WITH ENCLOSED TURNING VANES	67
A14.	YAW ANGLE DISTRIBUTION WITH ENCLOSED TURNING VANES	68
A15.	NON-DIMENSIONAL PRESSURE VS. BLADE-TO-BLADE LOCATION WITH ENCLOSED TURNING VANES AND $\beta = 39.2^\circ$	69
A16.	YAW ANGLE DISTRIBUTION WITH ENCLOSED TURNING VANES AND $\beta = 39.2^\circ$	70

ACKNOWLEDGMENT

The author would like to give special recognition to Tom and Diane McGuire without whose imaginative assistance, some of the photographs used in this report would not exist. Also, a special note of appreciation to Dr. R. P. Shreeve for the opportunity to work and study at the Turbopropulsion Laboratory.

I. INTRODUCTION

Codes and optimization techniques being developed for the design of modern compressor blades must incorporate a prediction of boundary layer transition and separation. The boundary layer calculation is an important part of the design method since the limit to be approached in the optimization procedure is the condition corresponding to insipient separation from the suction surface of the blade.

In a current study at the Turbopropulsion Laboratory of the Naval Postgraduate School, the performance of a proposed optimized controlled diffusion (CD) compressor stator blade shape is to be examined and compared with the performance of a double circular arc (DCA) blade shape which it has been designed to replace. The CD blade was designed as described in Reference 1, which incorporates a particular model for boundary layer transition. Both blade designs are being tested in a large subsonic cascade wind tunnel to obtain comparative blade element data at both on- and off-design conditions, surface pressure distribution data and detailed flow profiles for code verification.

In order to validate the optimization and flow analysis codes using test data, it is essential to establish experimentally the condition of the boundary layers when the test data are taken. In the work reported here, the china clay

technique was used for the first time in the subsonic cascade wind tunnel to determine transition and separation behaviors on blades under test. First, the technique itself was examined using a large flat plate china clay model mounted in the center of the test section and tested at varying Reynolds Numbers. The ability to interpret drying patterns on the plate surface when the leading edge was sharp, and when it was given a radius identical to that on the DCA blade, was developed. Secondly, the surface flow behavior on the DCA blades when operated over a range of incidence angles was examined and interpreted. It was concluded that the presence of a leading edge separation bubble at all incidence angles greater than -3° was sufficient to trigger transition and turbulent reattachment on the blade suction surface. Similar techniques will be applied in future tests of the CD blading, the leading edge of which has a larger radius and could lead to quite different results.

II. TEST FACILITIES AND INSTRUMENTATION

A. RECTILINEAR CASCADE

The cascade facility used in this study is shown in Figure 1. References 2 thru 4 describe the cascade and the modifications which preceded this study. Appendix A describes a further modification made to the plenum of the tunnel to reduce the turbulence level and possible excitation of the turning vanes. The cascade air supply is a 700 HP blower located in the basement of the cascade building. The test section is 10 x 60 inches and contains 20 test blades at preset incidence and stagger angles. The test section arrangement is shown in Figure 2. A plexiglas wall was used in place of the original steel wall to facilitate flow visualization techniques. The detailed measurement of flow conditions in the cascade test section were reported by Himes [Ref. 5]. Reference nominal flow velocities and Reynolds Numbers experienced at different power settings are listed in Table I.

B. INSTRUMENTATION

The complete tunnel instrumentation system was not required for this study. One DCA blade instrumented with 39 pressure taps as shown in Figure 3, was placed in the center of the cascade. A Prandtl probe was inserted into the flow three inches ahead of the test blades to measure reference

total and static pressures. All pressure measurements were recorded using a Hewlett-Packard 3052 Data Acquisition System and two 48 port Scanivalves. Pressure data were recorded and stored on magnetic tape cassettes.

C. CHINA CLAY TECHNIQUE

The emphasis in the present study was on the use of the china clay technique. The technique of applying a china clay coating to test models is described in Reference 6. Recommendation for the mixing of the china clay solution are also given in Reference 6, as well as some generalized guidelines for interpreting the surface patterns that develop.

The evaporation of the developer solution on the model surface is controlled by the laws of forced convective heat transfer. Briefly stated, the heat transfer rate, \dot{Q} , is given by

$$\dot{Q} = hA(T_f - T_s)$$

where h = convective surface heat transfer coefficient

A = surface area

T_f = bulk fluid temperature

T_s = solid body temperature

In the tests performed in the present study, the fluid temperature and the model temperature were nearly the same. Therefore, the parameter that controlled the evaporation of

the developer was the convective surface heat transfer coefficient, h .

The flat plate shown in Figure 4 was used to calibrate the observations. Figure 5 shows a schematic of the surface flow on a flat plate. As described in Reference 7, the laminar boundary layer has two subregions. The first region near the leading edge is characterized by a very high shear and a very thin boundary layer. The second region is characterized by a relatively thicker, well developed laminar boundary layer. The first region, because of the very high shear and very thin boundary layer, has a very high convective surface heat transfer coefficient. Therefore, on a china clay model, under a laminar boundary layer, the leading edge region will develop first.

The transitional and turbulent regions are characterized by high values of the convective surface heat transfer coefficient. The high value of h is due to the high transverse mixing and transport rates in turbulent regions. Figure 6 shows schematically the relative values of the convective surface heat transfer coefficient in different regions on a flat plate. Figure 6 was used as a guide in analyzing the surface patterns which developed on the test models.

A complication to the surface flow analysis is the unwanted existence of point turbulence generators. These are generally large china clay particles on the model

surface. They are readily detected as a result of the triangular pattern of dry surface which develops behind the particles. The disturbances are undesirable because they cause premature transition in the ideally two-dimensional surface boundary layer. Reference 8 details the effects of this type of disturbance.

D. TEST MODELS

The flat plate model was constructed of 7075-T6 aluminum with finished dimensions of 10 x 10 x 3/8 inches. One end, as shown in Figure 4, was machined to a sharp leading edge with a 7° ramp angle. The opposite end was machined with a leading edge radius of 0.044 inch and a 7° ramp angle. The model was then black anodized prior to mounting the shank.

The DCA blade model was cast of an aluminum-filled epoxy using an original blade as a master. Because the epoxy was not strong enough itself to withstand the blade loads, a steel backbone 0.063 inch thick and 1.5 inches wide was molded into the blade the entire length of the span. The epoxy was dark enough when cast to make additional darkening agents unnecessary.

Both models were built with detachable aluminum shanks. The shanks were pinned to a tongue which was an integral part of the model. With the model and shanks assembled, a china clay coating was applied following the description in Reference 6.

E. TEST PROCEDURE

The process for using the china clay technique required the cascade test section wall to be removed prior to spraying the methyl salycilate developer on the test model. Care was taken to keep the developer layer as thin as possible. It was found that a gentle blotting of the surface with a clean paper towel did not adversely affect the tests or the china clay surface and helped to keep the developer layer uniformly thin. The test section wall was then replaced and the test performed.

The drying process on the model surface was dependent on the flow velocity. For example, at flow velocities on the order of 100 feet per second, the DCA blade would develop the transition pattern in approximately three minutes; at 200 feet per second the transition pattern would appear in less than a minute. This meant that at the higher Reynolds Numbers the surface drying patterns would change very quickly. Visual observation and still photographs were made, however, the motion pictures made of the drying process were the most useful. The motion picture camera, however, required the most care in the control of lighting and camera angles.

III. TEST PROGRAM AND RESULTS

A. OUTLINE OF TESTS

The present study was conducted in two phases. The first phase was to mount the flat plate model alone in the center of the cascade with a straight-through passage and to run it with the same inlet flow conditions as for the DCA blades. This provided a means of "calibrating" the china clay visualization technique to be use on the DCA blades. Additionally, leading edge radius effects could be examined without the influence of blade curvature.

The second phase was the study of the surface flow over the DCA blades. Emphasis was placed on obtaining visual evidence of transition and separation over a range of incidence angles and Reynolds Numbers. Surface pressures were also obtained.

B. TEST PROGRAM

The flat plate was placed in the cascade with the sharp leading edge forward such that the flow incidence angle to the flat surface was -0.5° . This was done to insure that there would be no leading edge separation. Three tests were conducted at three different Reynolds Numbers (based on plate length) ranging from 0.5×10^6 to 1.25×10^6 . Observations of the high shear regions of the laminar boundary

layer and movement of the transition location were made. Figure 7 is a representative example of the drying patterns observed on the flat plate. The transition points on the flat plate and the Reynolds Numbers at which they occurred are shown in Figure 8. Transition was determined to have occurred when three conditions were met: 1) a region of rapid drying occurred near the leading edge, 2) a region of surface drying developed farther downstream on the blade after the leading edge region developed, and 3) there was no separation bubble near the leading edge. The measurement of the transition point was made at the leading edge of the second region of surface drying once that region had completed a rapid, erratic three-dimensional development and had just begun to move two-dimensionally towards the leading edge. One test was then conducted with the flow incidence angle to the flat surface set at $+0.5^{\circ}$ to examine the visual appearance and sensitivity of the flow to leading edge separation.

The flat plate was then placed in the flow with the rounded leading edge forward. Three tests were conducted with the flow incidence angle to the flat surface ranging from -4° to $+4^{\circ}$. The flow velocity was the same for the three tests. Figure 9 shows examples of the photographic results of the three tests. The transition point as well as the leading edge separation and reattachment point for the three tests are shown in Figure 10.

The DCA blade cascade was configured to have the parameters given in Table II. The five flow incidence angles used by Cina [Ref. 9] were set in turn. At each flow incidence angle, three tests were conducted at Reynolds Numbers based on chord length ranging from 0.3×10^6 to 0.8×10^6 . Photographic records of the china clay observations are presented in Figure 11. Surface pressure data were recorded, converted to velocities, and are presented in Figure 12. Transition, separation and reattachment points deduced from the observations are shown in Figure 13.

IV. DISCUSSION

A. FLAT PLATE EXPERIMENTS

The flat plate was designed to have some of the same features as the DCA blade. For example, the ramp angle of 7° on the flat plate approximated the angle between the suction and pressure surfaces on the leading edge of the DCA blade, and the rounded leading edge was identical to the leading edge of the DCA blade. The length of 10 inches was chosen to insure sufficient chord length for transition to occur.

The tests with the sharp leading edge forward and -0.5° incidence angle, Figure 7, clearly showed that transition occurred in an irregular pattern and that the region of high shear laminar boundary layer covered approximately one quarter of the laminar boundary layer region. Shown in Figure 8, transition Reynolds Numbers were relatively constant at approximately 0.82×10^6 . Since the transition region on a flat plate under good wind tunnel conditions is recognized to occur at Reynolds Numbers of 0.3 to 0.5×10^6 , indications are that the flow has very low turbulence and that the china clay surface did not introduce any critical flow disturbances.

With the rounded leading edge forward and positive incidence angles, a definite separation bubble appeared on

the flat plate. At -1° and -3° incidence angles to the flat plate surface the separation bubble persisted. At -4° , however, the flat plate again presented the same surface drying patterns as the flat plate with the sharp leading edge and -0.5° incidence angle. Since -3.5° incidence to the flat surface was equivalent to 0° incidence to the effective "camber line" at the leading edge, the flow saw a lifting surface near the leading edge at all incidence angles greater than -3.5° . This implies the occurrence of a favorable pressure gradient from the stagnation point followed by an adverse pressure gradient around the remainder of the leading edge to the suction surface. Reference 8 indicates that adverse pressure gradients as low as 5% were sufficient to cause the surface flow to transition to turbulent. Therefore, for the incidence angles to be examined in this study and the leading edge radius to be used, turbulent flow over the major part of the surface might be expected to occur for incidence angles greater than -3.5° .

The question of whether the flow after the separation bubble reattaches lamina rly or turbulently was resolved by comparison of the drying rates in the corners with those along the center of the blade. Since the corner flow was turbulent, a centerline flow that produced a dry surface pattern at the same rate as the corners must have had a similar value of h and therefore probably have been

similarly turbulent. Based on this argument, in all tests with a leading edge separation bubble, the flow reattached turbulently.

B. DCA BLADE EXPERIMENTS

The results of the DCA blade experiments could be interpreted following the experience established using the flat plate model. Many effects were similar to the flat plate with a rounded leading edge. As is consistent with the pressure distributions in Figure 12, for positive incidence angles there existed a separation bubble at the leading edge with a turbulent reattachment. Turbulent reattachment was again determined by comparing the drying rates in the corners with the centerline drying rates. At negative flow incidence angles less than -3.5° , the flow over the suction surface was laminar with transition occurring at approximately 80% chord (see Figures 11d and 11e). Trailing edge separation on the suction side was not pronounced for the tests at negative incidence angles. For the two negative incidence angles, the suction surface trailing edge separation point was relatively constant at 96% chord. This behavior at negative incidence angles is evidenced in Figure 12 by the "plateau" like behavior of the pressure profile.

It should be noted that the trailing edge separation points were difficult to define precisely because of an

accumulation of developer liquid under gravity in regions of separation. This would cause premature separation, as the fluid must be supported by the flow. Consequently, an estimate and not a measurement of the point of separation was made. These estimates were plotted in Figure 13 and show the approximate movement of the separation points with variation in incidence angle.

The results in Figure 13 would suggest that there might be qualitative differences in the behavior of the blade losses as incidence is changed for incidence angles greater than 2.1° compared to those for incidence angles less than -4.9° . Such a difference was found by Himes and can be seen in Figure 9 of Reference 5.

V. CONCLUSIONS

The following conclusions were drawn concerning the DCA blade boundary layer:

1. At flow incidence angles between 2.1° and 8.9° , the boundary layer separated very near the leading edge, transitioned to turbulent flow, and reattached immediately downstream on the suction surface of the blade. The exact point of reattachment was controlled by the incidence angle.
2. At flow incidence angles less than -4.9° , a laminar boundary layer existed over most of the suction surface and transition occurred at approximately 80% chord depending on incidence angle and blade chord Reynolds Number.
3. Trailing edge separation was observed on the suction surface at all incidence angles. The movement of the separation point went from approximately 96% chord at -9.2° incidence angle to 84% chord at 8.8° incidence angle.
4. Tests at several incidence angles between -4° and -12° are necessary to completely define the blading performance.

TABLE I

NOMINAL FLOW VELOCITY AND TEST REYNOLDS NUMBERS

FLAT PLATE

SETTING	APPROX. VELOCITY	Re_c
LOW	114 ft/sec	0.6×10^6
MED	162 ft/sec	0.8×10^6
HIGH	204 ft/sec	1.1×10^6

DCA BLADE

SETTING	APPROX. VELOCITY	Re_c
LOW	114 ft/sec	0.3×10^6
MED	162 ft/sec	0.4×10^6
HIGH	204 ft/sec	0.5×10^6

TABLE II
DCA BLADE CASCADE CONFIGURATION

NO. of BLADES	20
SOLIDITY	1.67
STAGGER ANGLE	14.27
SPACING	3.0
CAMBER ANGLE	45.72
CHORD	5.01
THICKNESS (% chord)	7

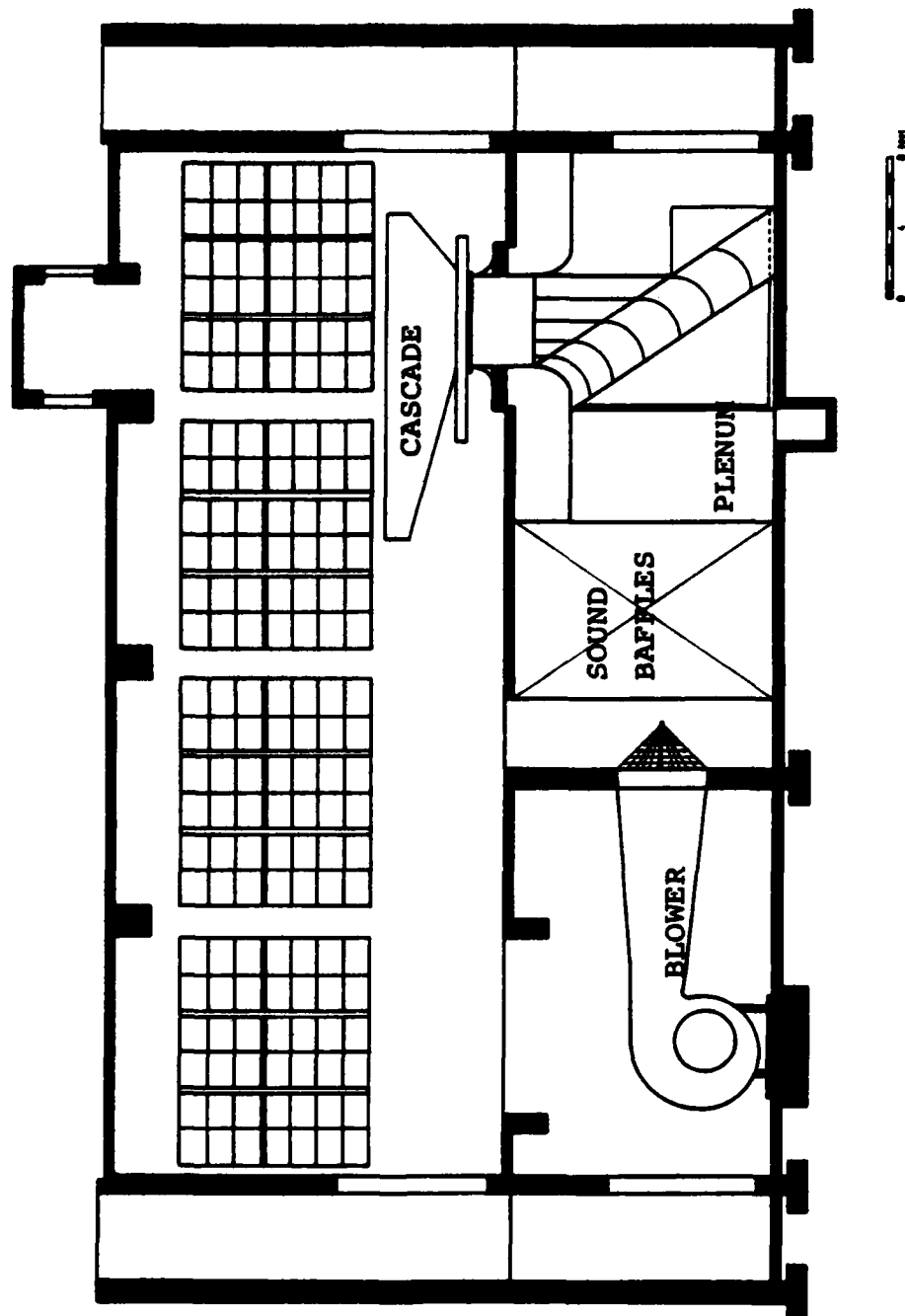


FIGURE 1. CASCADE WIND TUNNEL TEST FACILITY.

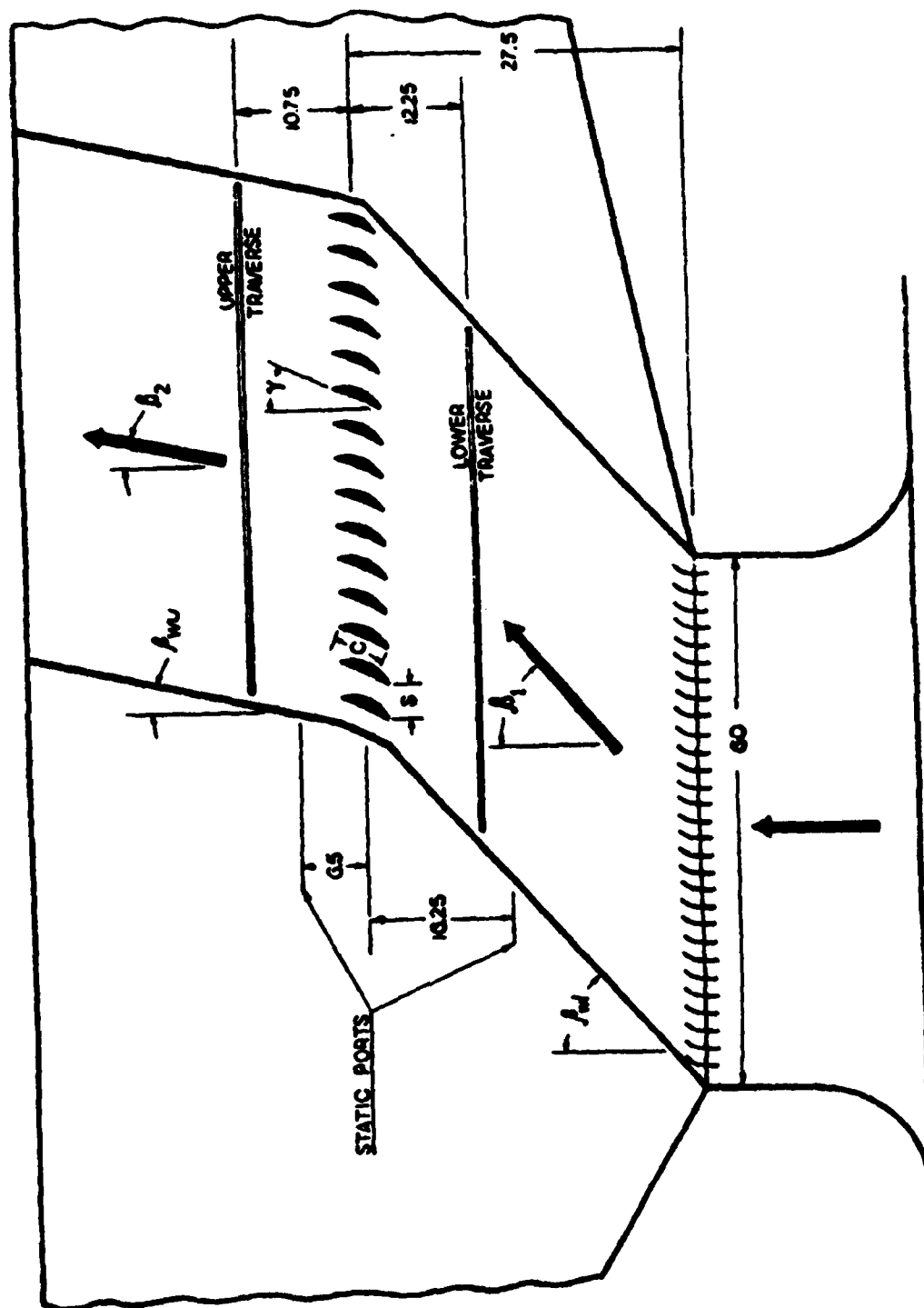


FIGURE 2. CASCADE TEST SECTION SCHEMATIC.

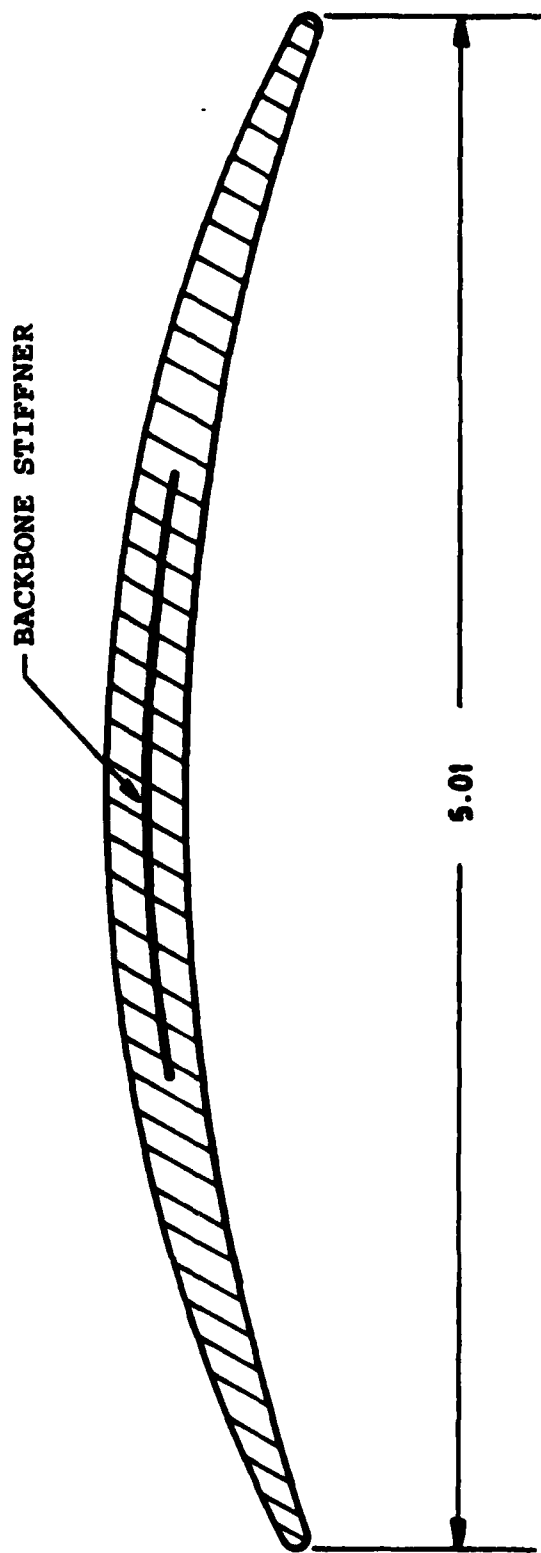


FIGURE 3. DCA BLADE PROFILE.

SHARP EDGE

ROUNDED EDGE
(RADIUS = 0.044)

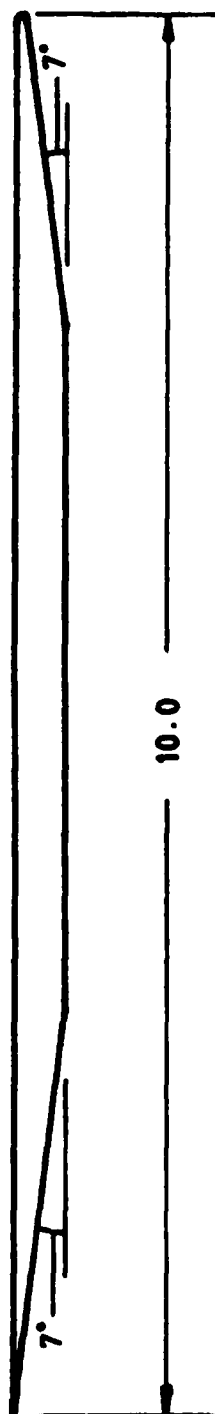
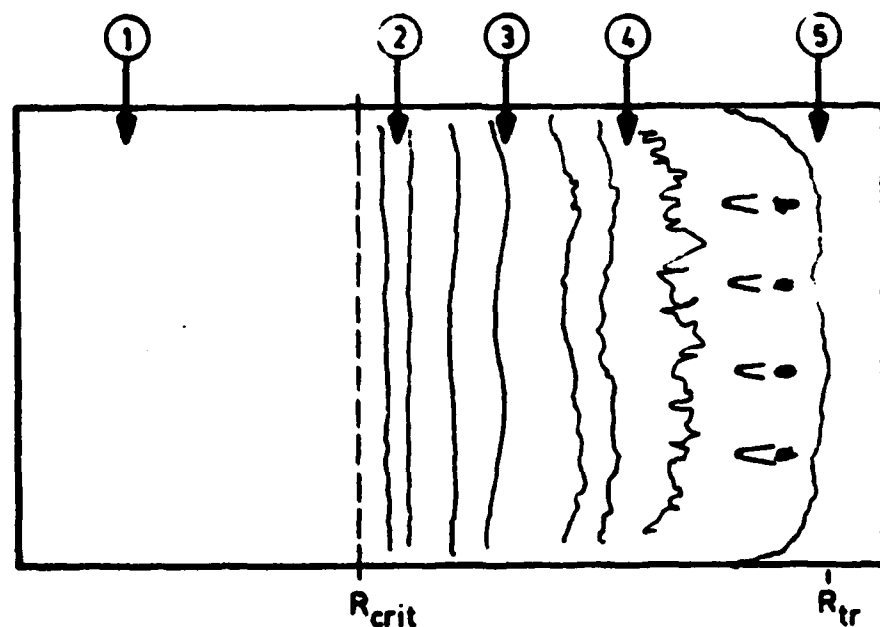


FIGURE 4. FLAT PLATE PROFILE.



1. STABLE FLOW
2. UNSTABLE TOLLMEIN-SCHLICHTING WAVES
3. 3-D WAVES AND VORTEX FORMATION
4. BURSTING OF VORTICES
5. FULLY TURBULENT FLOW

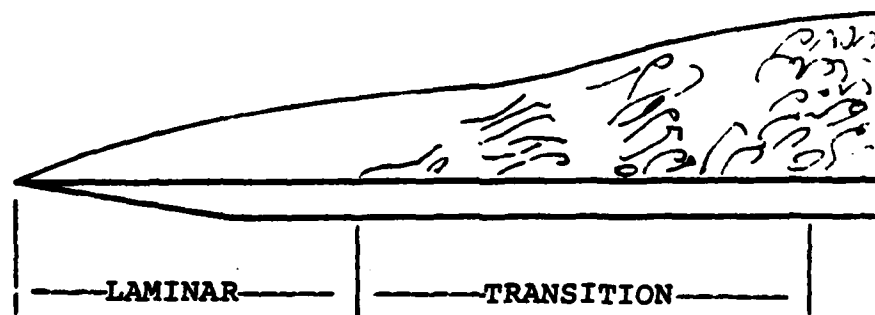


FIGURE 5. FEATURES OF BOUNDARY LAYER FLOW ON FLAT PLATE AT 0° INCIDENCE.

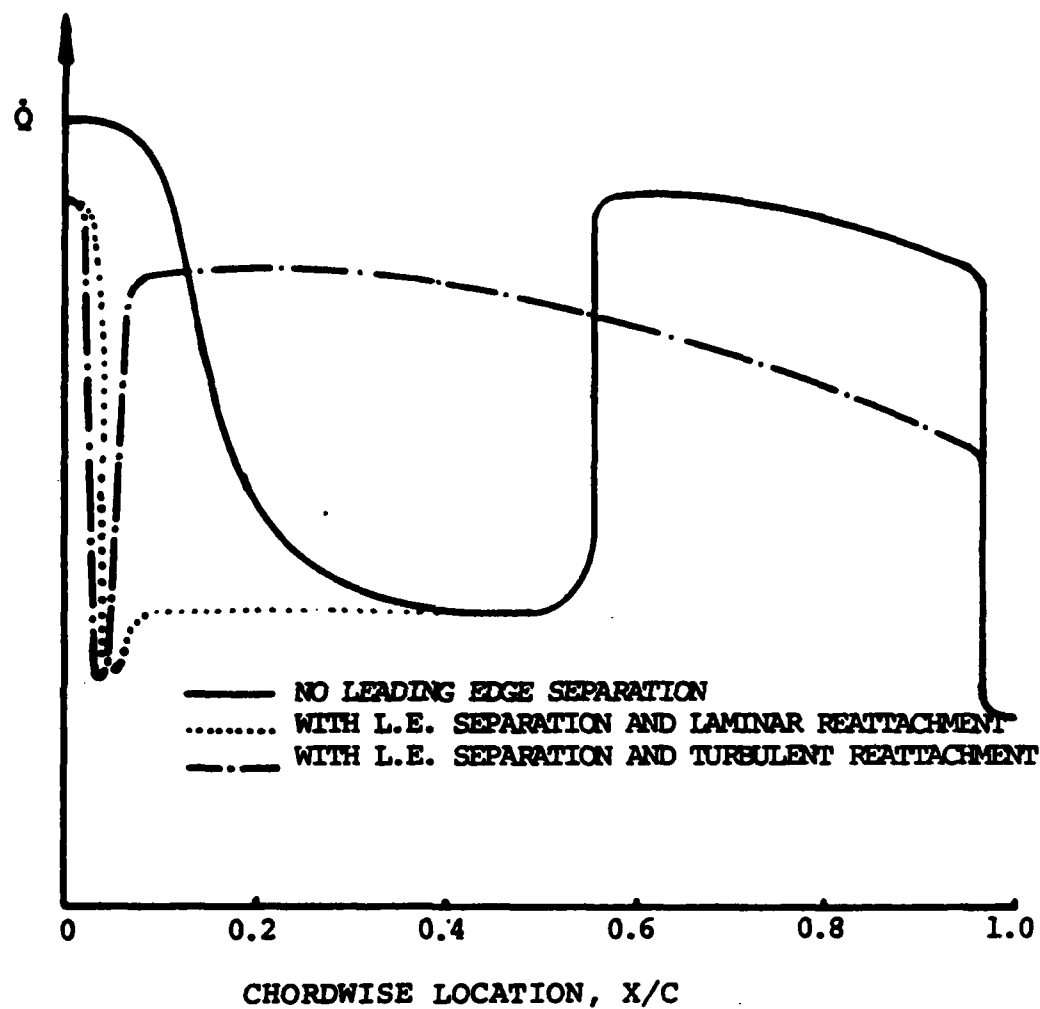


FIGURE 6. RELATIVE VALUES OF SURFACE HEAT TRANSFER RATES UNDER DIFFERENT FLOW CONDITIONS.

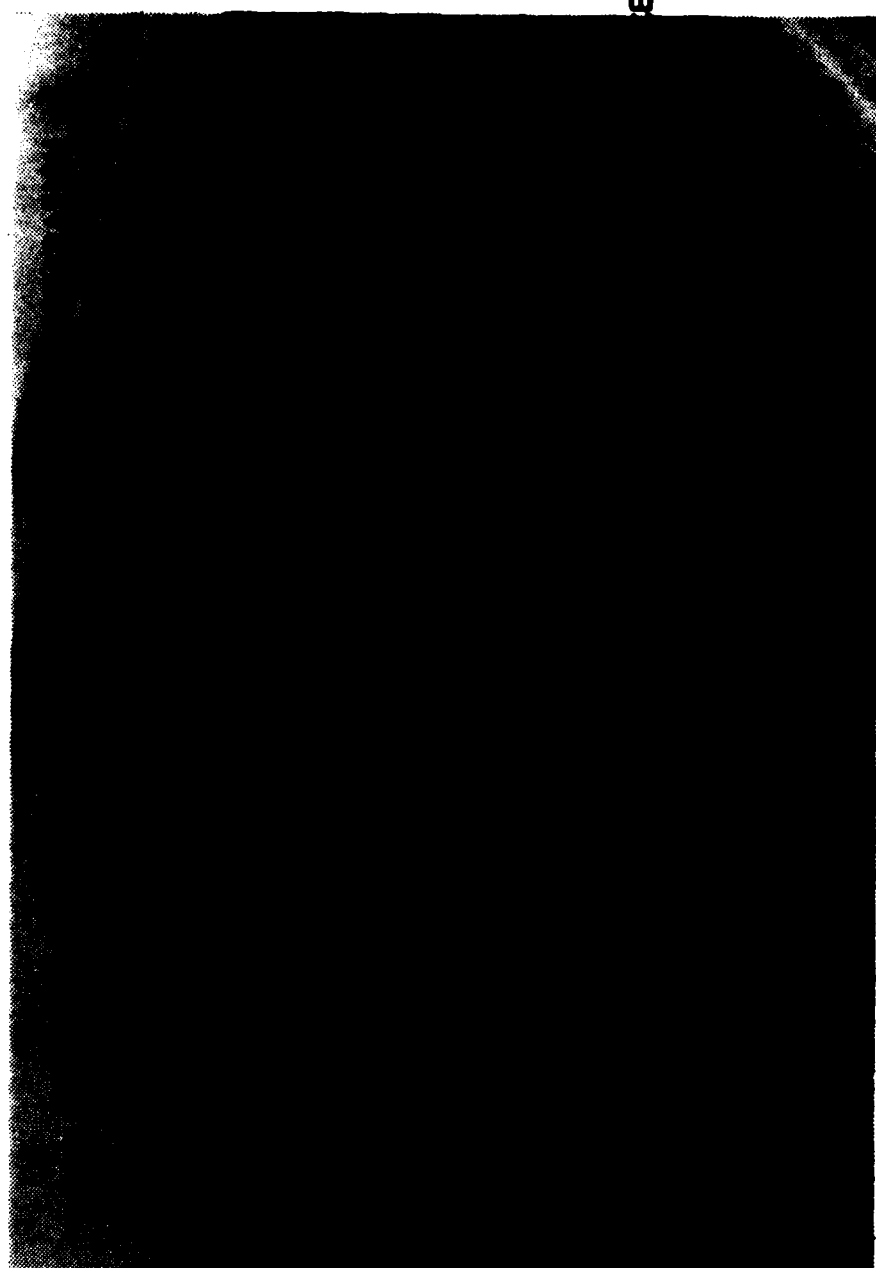


FIGURE 7. DRYING PATTERNS ON A FLAT PLATE WITH A SHARP LEADING EDGE ($i = -0.5^{\circ}$).

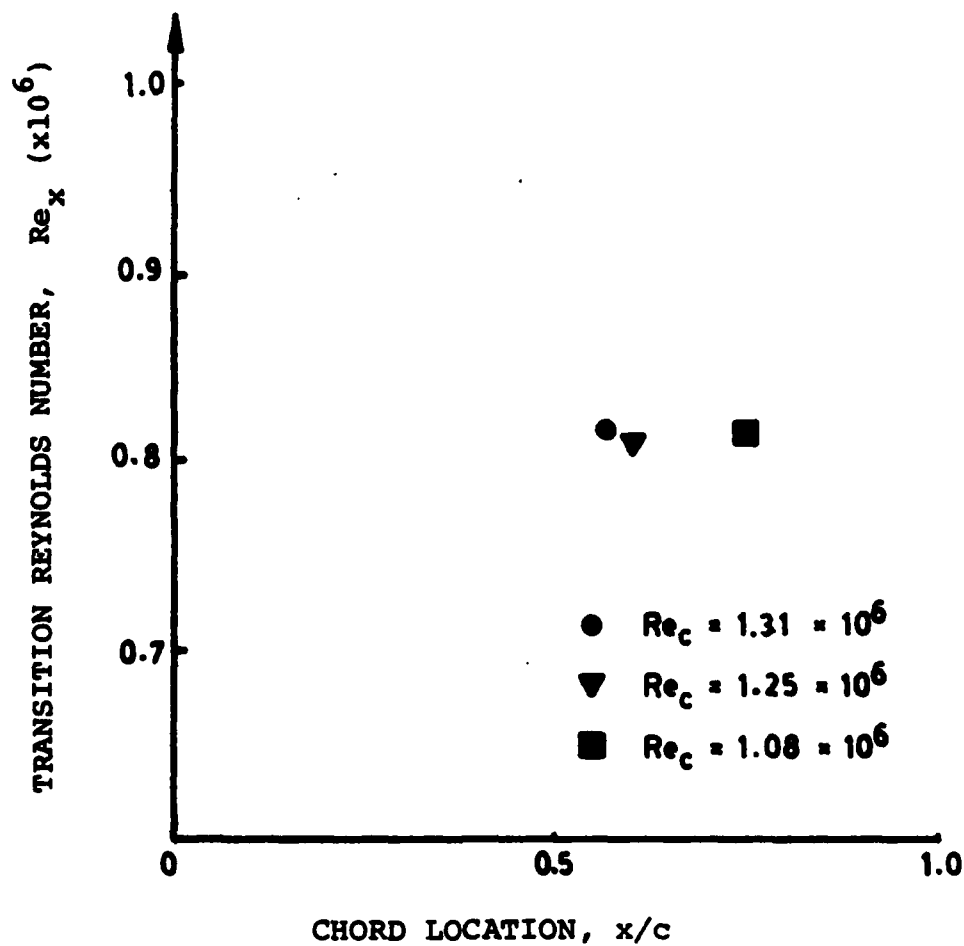


FIGURE 8. TRANSITION LOCATION VS REYNOLDS NUMBER FOR FLAT PLATE.



FIGURE 9a. SURFACE FLOW PATTERNS AT -4° INCIDENCE
ON A FLAT PLATE WITH ROUNDED LEADING EDGE.

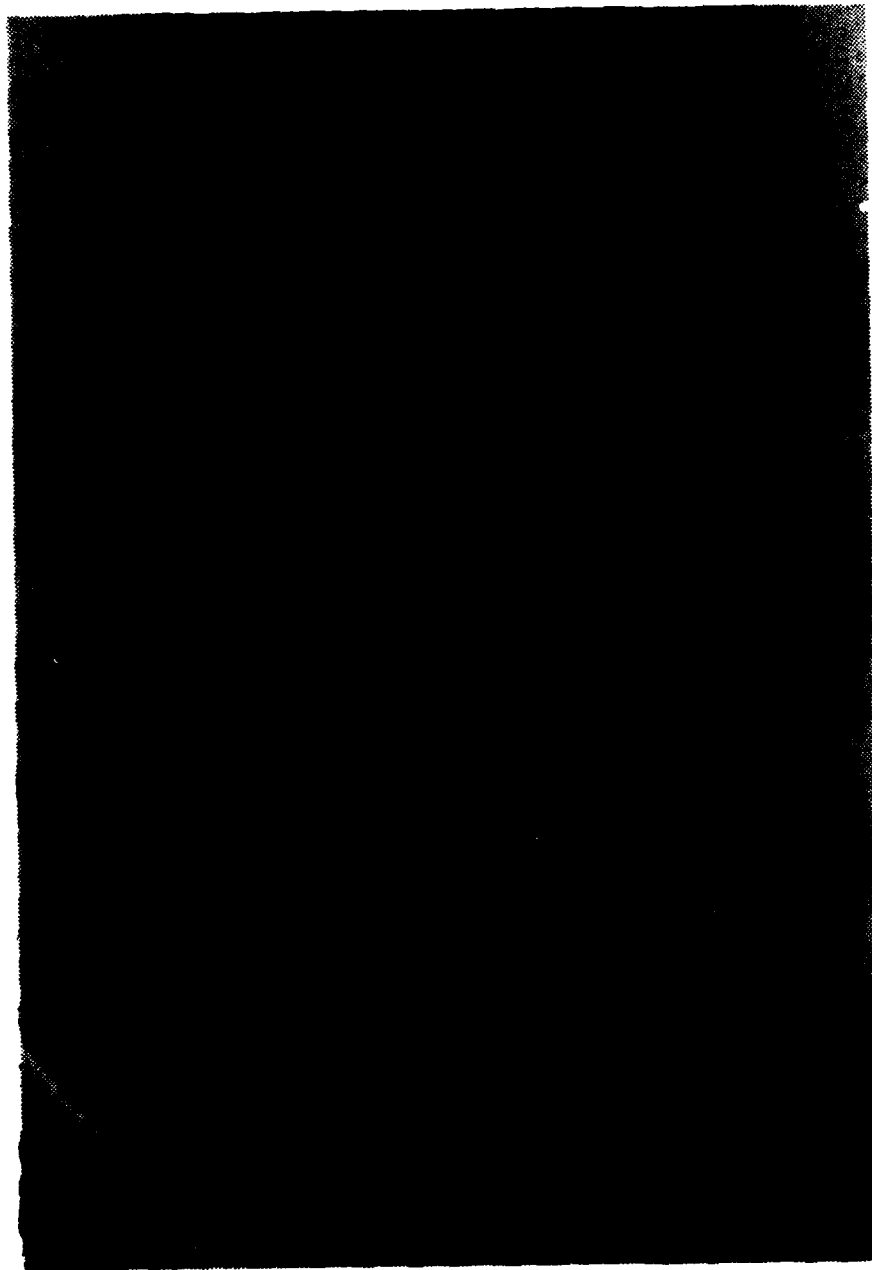


FIGURE 9b. SURFACE FLOW PATTERN AT 0° INCIDENCE ON A FLAT
PLATE WITH A ROUNDED LEADING EDGE.

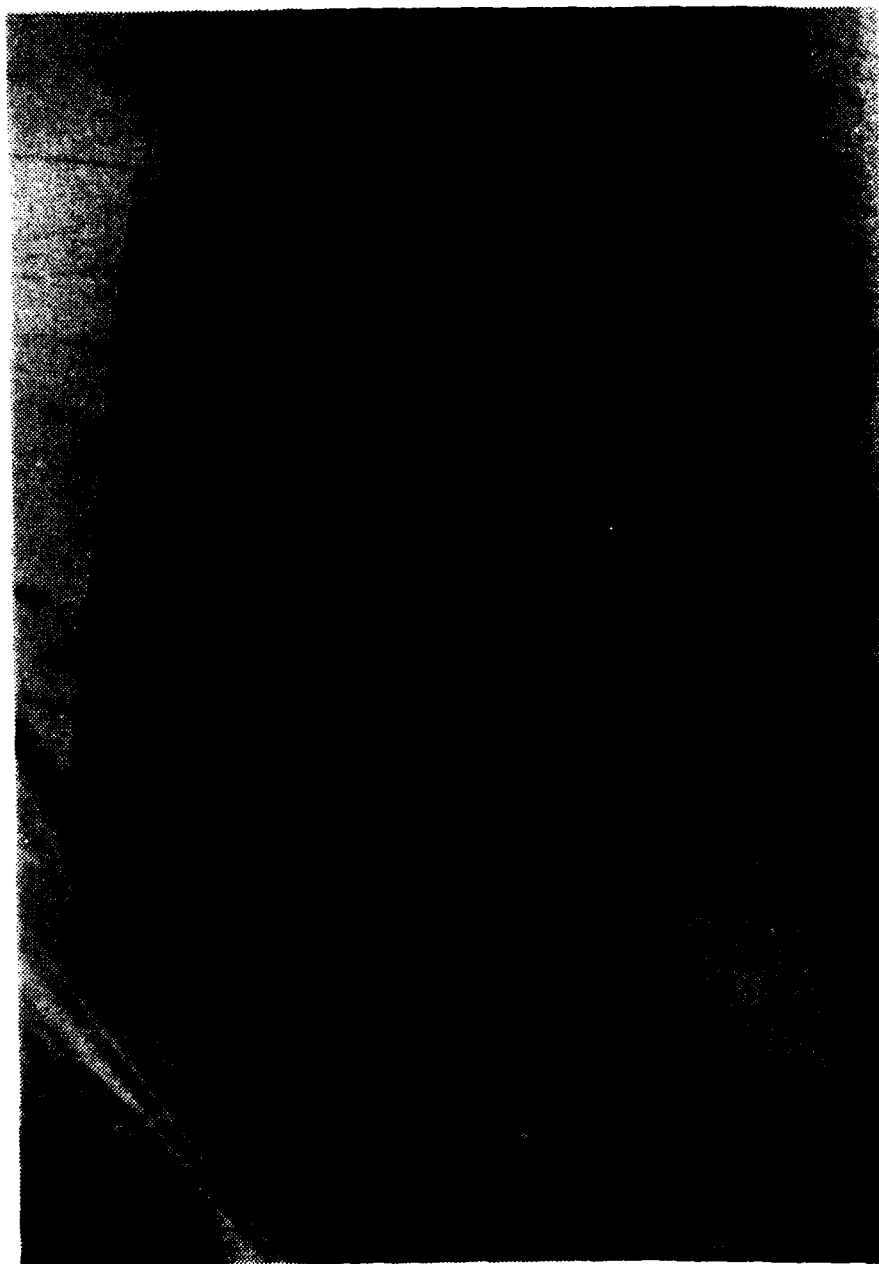


FIGURE 9c. SURFACE FLOW PATTERN AT 4° INCIDENCE ON A FLAT
PLATE WITH A ROUNDED LEADING EDGE.

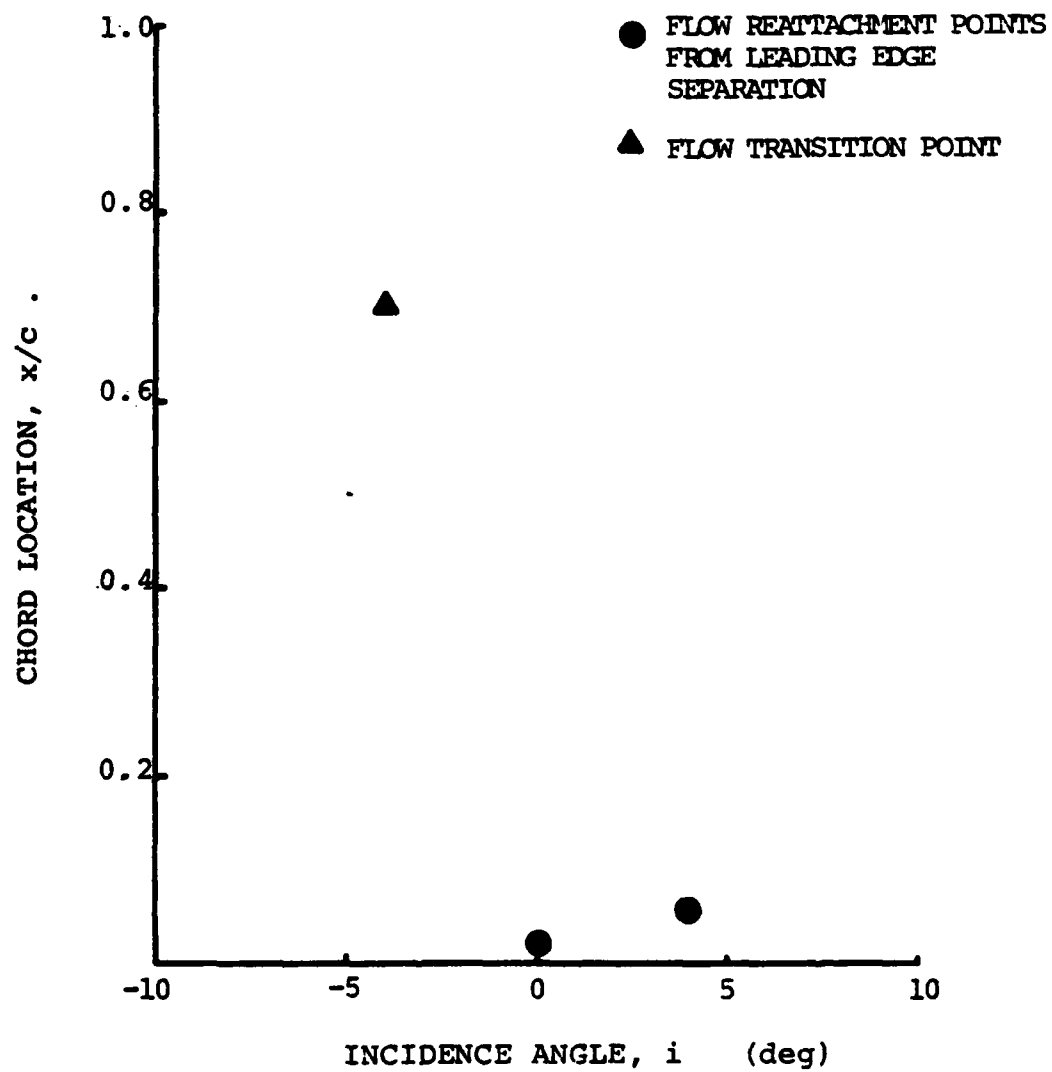


FIGURE 10. TRANSITION AND REATTACHMENT POINTS VS. INCIDENCE FOR FLAT PLATE WITH ROUNDED LEADING EDGE



FIGURE 11a. SURFACE FLOW PATTERN ON DCA BLADE, $i = 8.8^\circ$

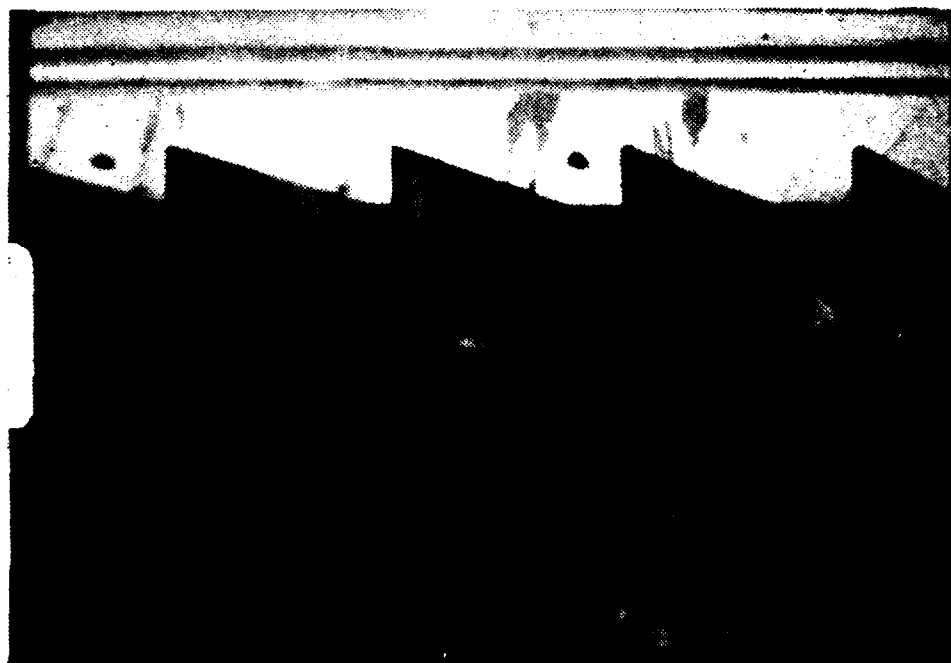


FIGURE 11b. SURFACE FLOW PATTERN ON DCA BLADE, $i = 5.3^\circ$



FIGURE 11c. SURFACE FLOW PATTERN ON DCA BLADE, $i = 2.1^\circ$



FIGURE 11d. SURFACE FLOW PATTERN ON DCA BLADE, $i = -4.9^\circ$



FIGURE 11e. SURFACE FLOW PATTERN ON DCA BLADE, $\alpha = -9.2^\circ$

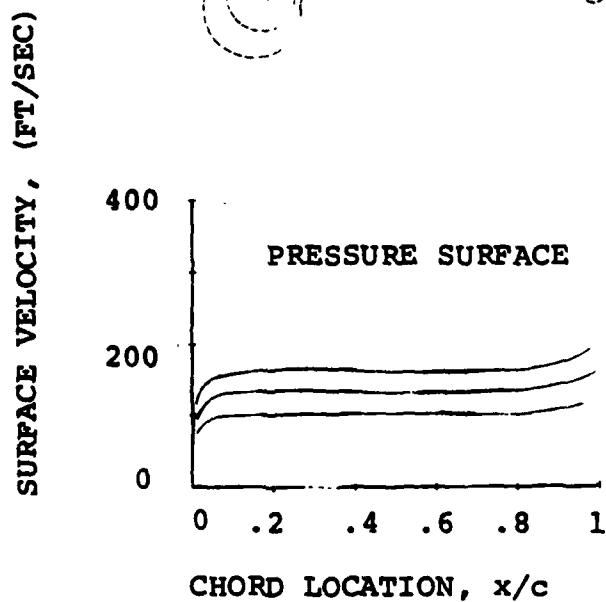
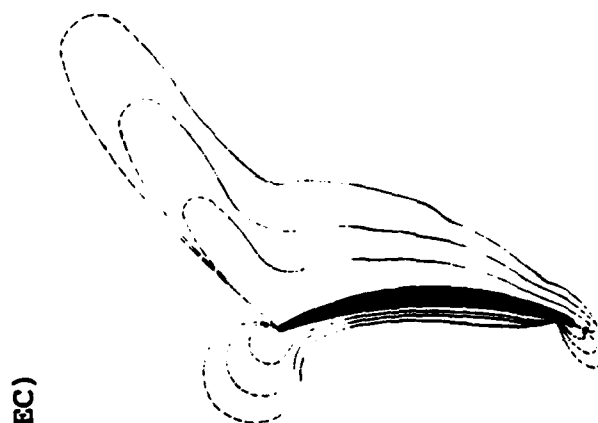
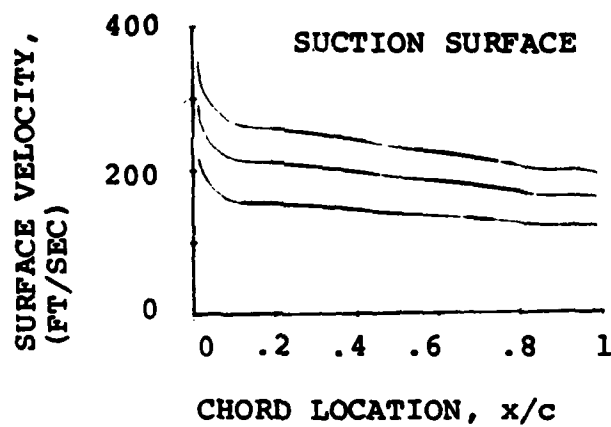


FIGURE 12a. PRESSURE AND VELOCITY DISTRIBUTION ON THE DCA BLADE, $i = 8.8^\circ$.

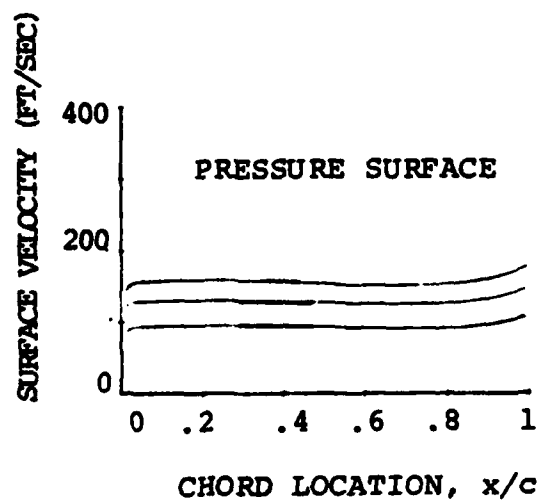
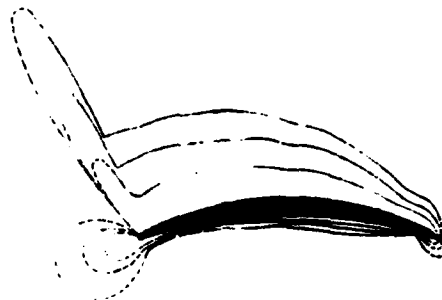
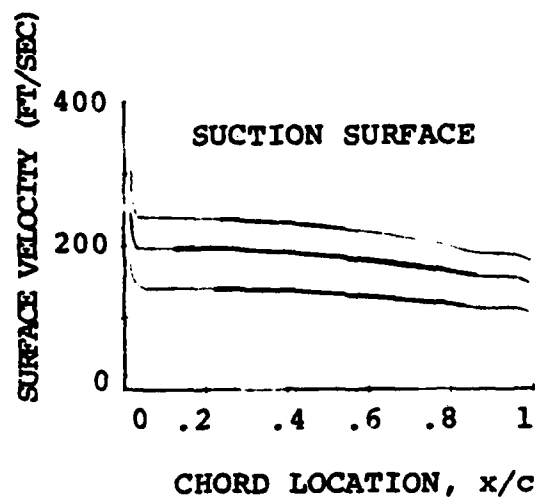


FIGURE 12b. PRESSURE AND VELOCITY DISTRIBUTIONS ON THE DCA BLADE, $i = 5.3^\circ$

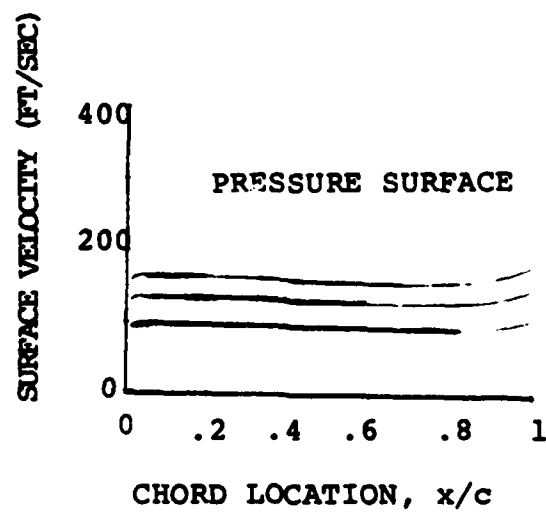
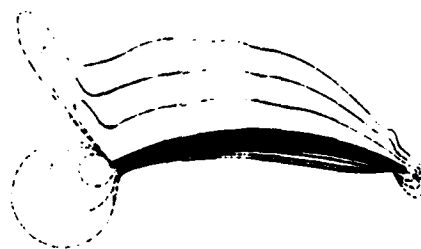
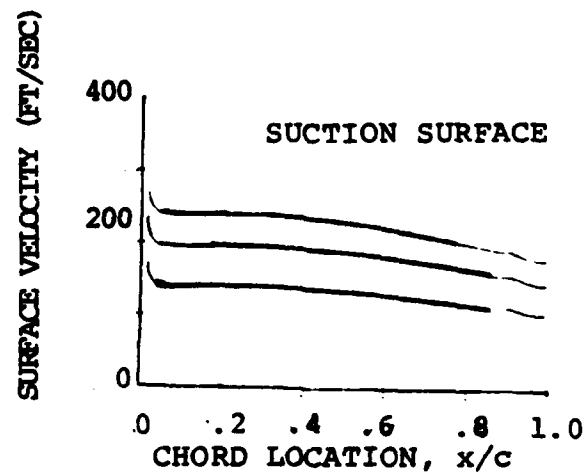


FIGURE 12c. PRESSURE AND VELOCITY DISTRIBUTION ON THE DCA BLADE, $i = 2.1^\circ$.

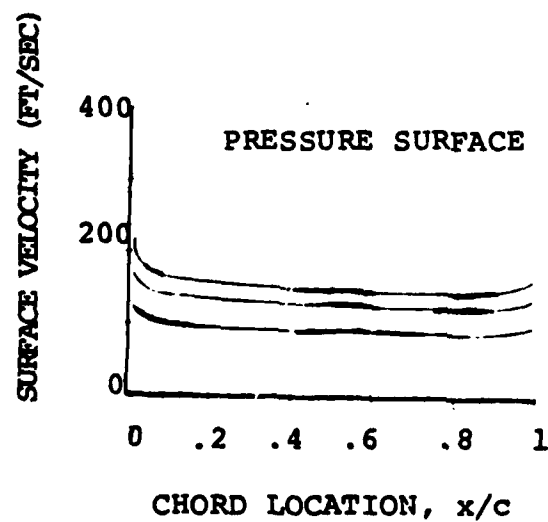
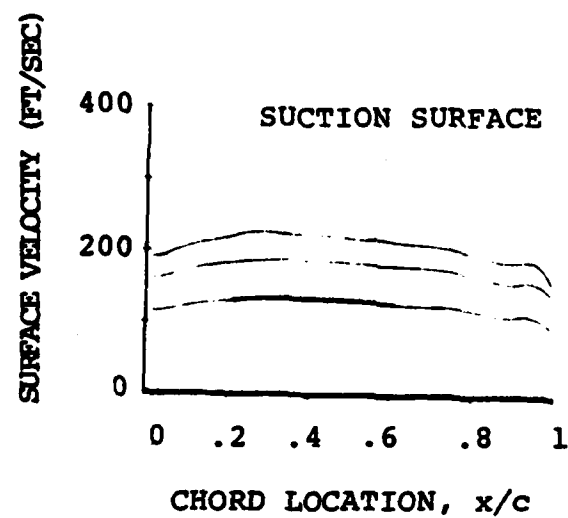


FIGURE 12d. PRESSURE AND VELOCITY DISTRIBUTION ON THE DCA BLADE, $i = -4.9^\circ$.

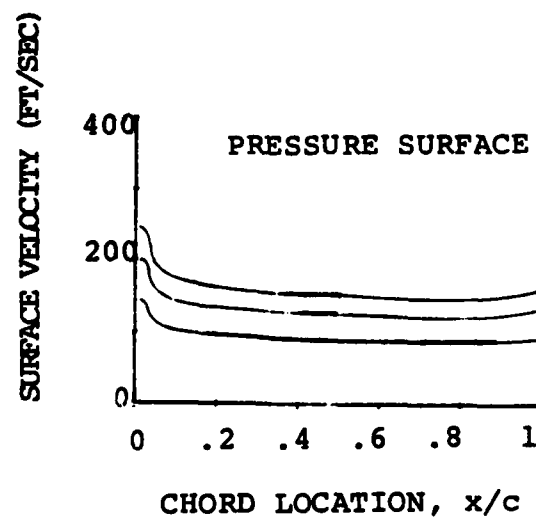
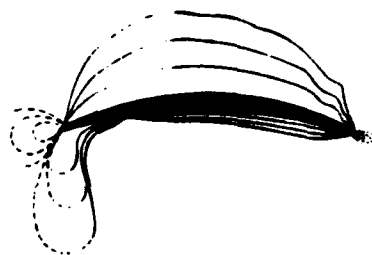
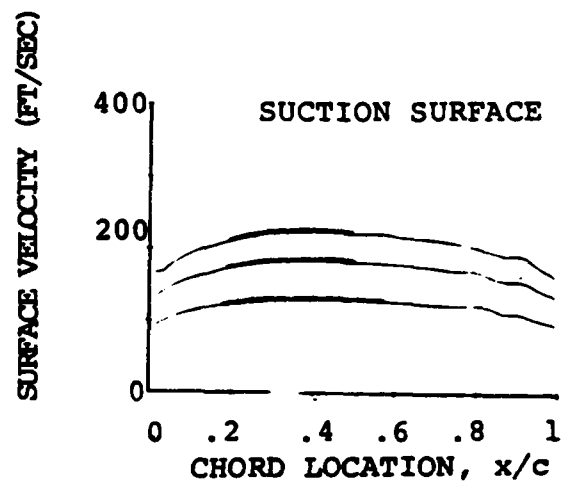


FIGURE 12e. PRESSURE AND VELOCITY DISTRIBUTION ON THE DCA BLADE; $i = 9.1^\circ$.

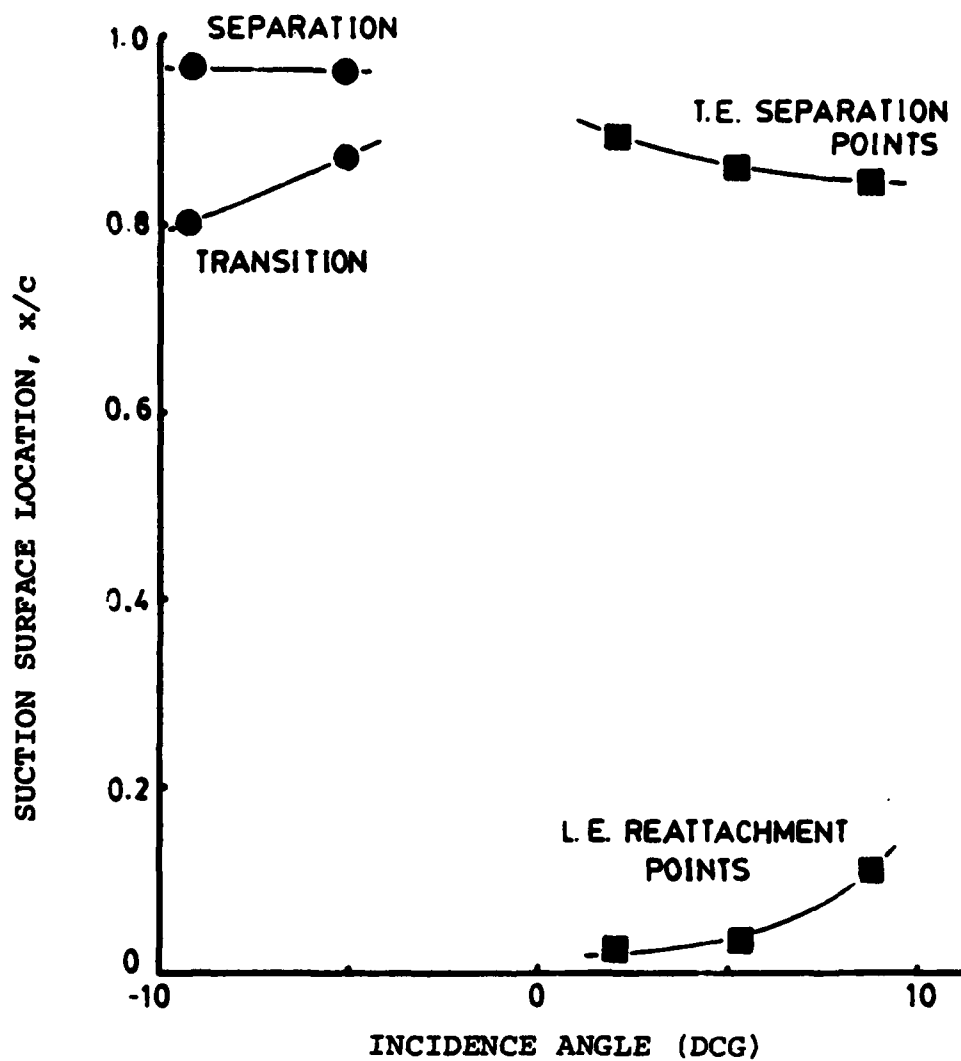


FIGURE 13. DCA BLADE SUCTION SURFACE FLOW CHANGES WITH INCIDENCE ANGLE ($Re \approx .4 \times 10^6$).

APPENDIX A: PLENUM MODIFICATION

The plenum configuration described by Moebius [Ref. 4] introduced large scale unsteadiness into the flow in the process of solving an initial problem of gross non-uniformity in time average flow. When near failure of the inlet guide vanes occurred following a redesign of this section [Ref. 10], the flow fluctuations made a diagnosis difficult and may have contributed to the problem. In the redesign of the guide vane section, two sets of right and left handed vanes were alternately cantilevered from opposite sides of the cascade to form a complete array of vanes at one inch spacing. After the modification was completed, the flow into the test cascade was found to be unsatisfactory and the adequacy of the plenum arrangement was again questioned. The flow conditions into the plenum chamber through the sound baffles (Fig. 1) which were present at that time are qualitatively shown in Figure A1. The pressure distribution and yaw angle variation for the region downstream of the inlet guide vanes into the test cascade are also shown in Figures A2 and A3, respectively.

To remove the cause of fluctuations in the plenum the baffles and diverter plates (Fig. 1) were removed. As shown

in Figures A4 and A5, this had a negative effect on the distributions into the cascade test section, although the steadiness was much improved.

Based on the prevailing conditions recorded in Figures A1, A4 and A5, modification of the plenum from the blower exit to the inlet guide vanes was attempted. First, the screens on the west end of the sound baffles were removed. A diffusing screen arrangement shown in Figure A6, was then placed over the blower exit. A more even distribution of flow from the sound baffles was realized, as shown in Figure A7.

Next, an array of turning vanes fabricated from materials used earlier by Bartocci [Ref. 3] was put into the plenum chamber. The configuration of that array is shown in Figure A8. The array was designed according to methods described by Idel'chik [Ref. 11]. The number of vanes was determined by the equation

$$n_{\text{opt}} = 1.4 \left(\frac{D_H}{r} \right)$$

where D_H = hydraulic diameter

r = radius of curvature

n_{opt} = optimum number of blades.

The spacing of the blades was important and was arrived at by using the following equation from Reference 11;

$$a_i = 0.67 \frac{s}{n+1} \left(1 + \frac{i-1}{n}\right)$$

where s = overall length of the turning vane array

n = number of blades in the array

i = specific blade number, 1,2,3,... n

a_i = spacing for 'ith' blade number.

Following the installation of the vanes, pressure and flow yaw angle data were recorded and are presented in Figures A9 and A10. An improvement in time-mean conditions resulted, however, it was noted that flow in the plenum was still not as stable as was desired. It was found experimentally that the flow coming out of the turning vanes had a vortex and eddying motion such as that depicted in Figure A11.

To eliminate this vortex production a total enclosure of the turning vanes was constructed. Figure A12 shows a sketch of the enclosed turning vanes. Figures A13 and A14 show the resulting pressure and flow yaw angle distributions.

With the plenum in its final form, the total pressure was shown (Fig. A15) to vary less than 4% over the span of the cascade with the walls at 39.2° and the flow yaw angle to vary $\pm 0.75^\circ$, (Fig. A16).

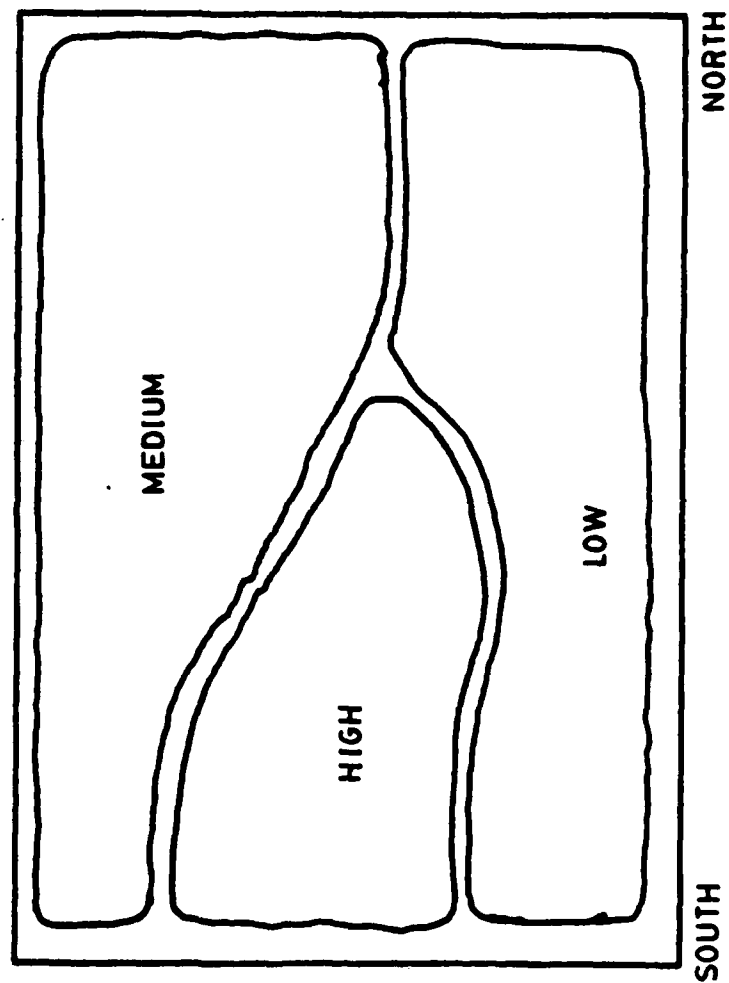


FIGURE A1. RELATIVE VELOCITIES EXITING SOUND BAFFLES
PRIOR TO MODIFICATION.

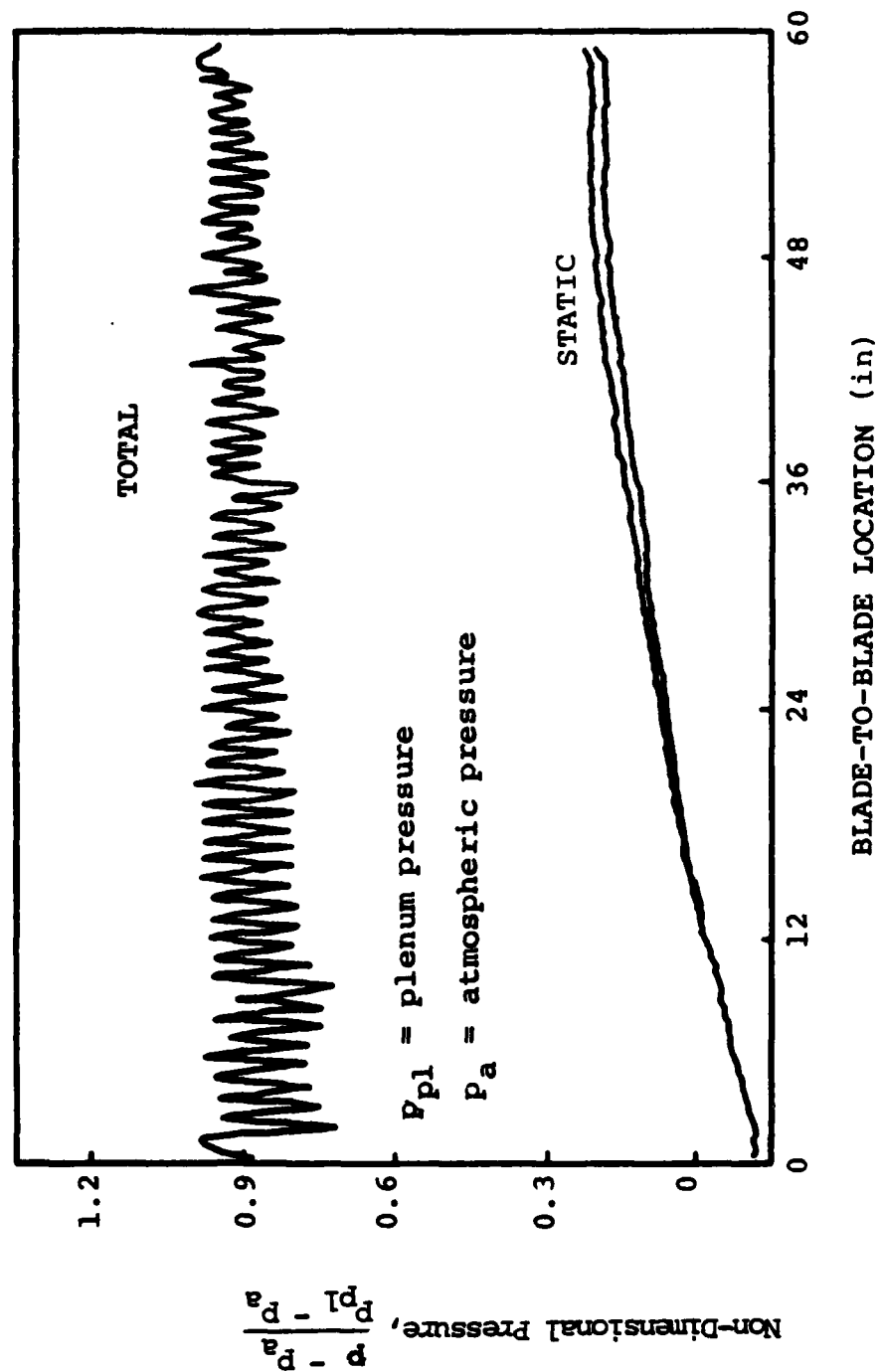


FIGURE A2. NON-DIMENSIONAL PRESSURE VS. BLADE-TO-BLADE LOCATION WITH BAFFLES AND DIVERTER PLATE IN PLENUM. (1/4 inch intervals)

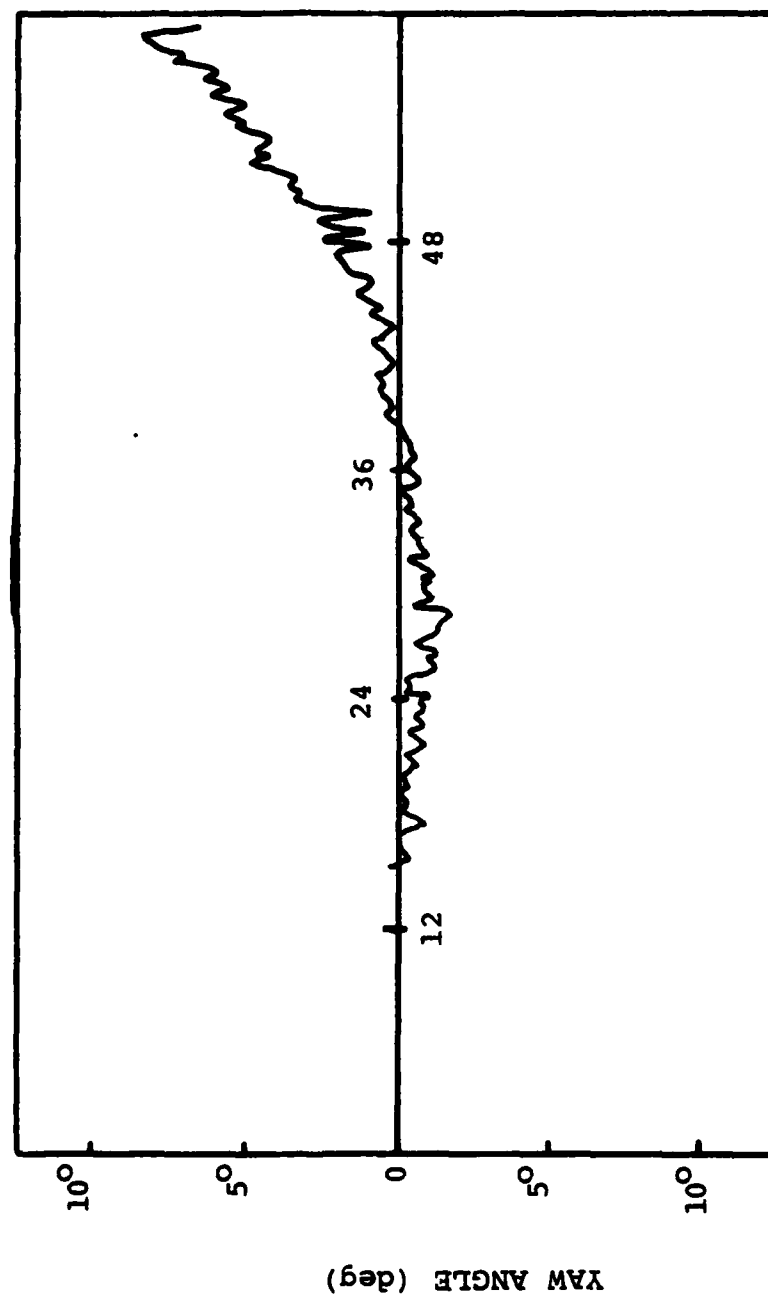


FIGURE A3. YAW ANGLE DISTRIBUTION WITH BAFFLES AND DIVERTER PLATE IN THE PLENUM.

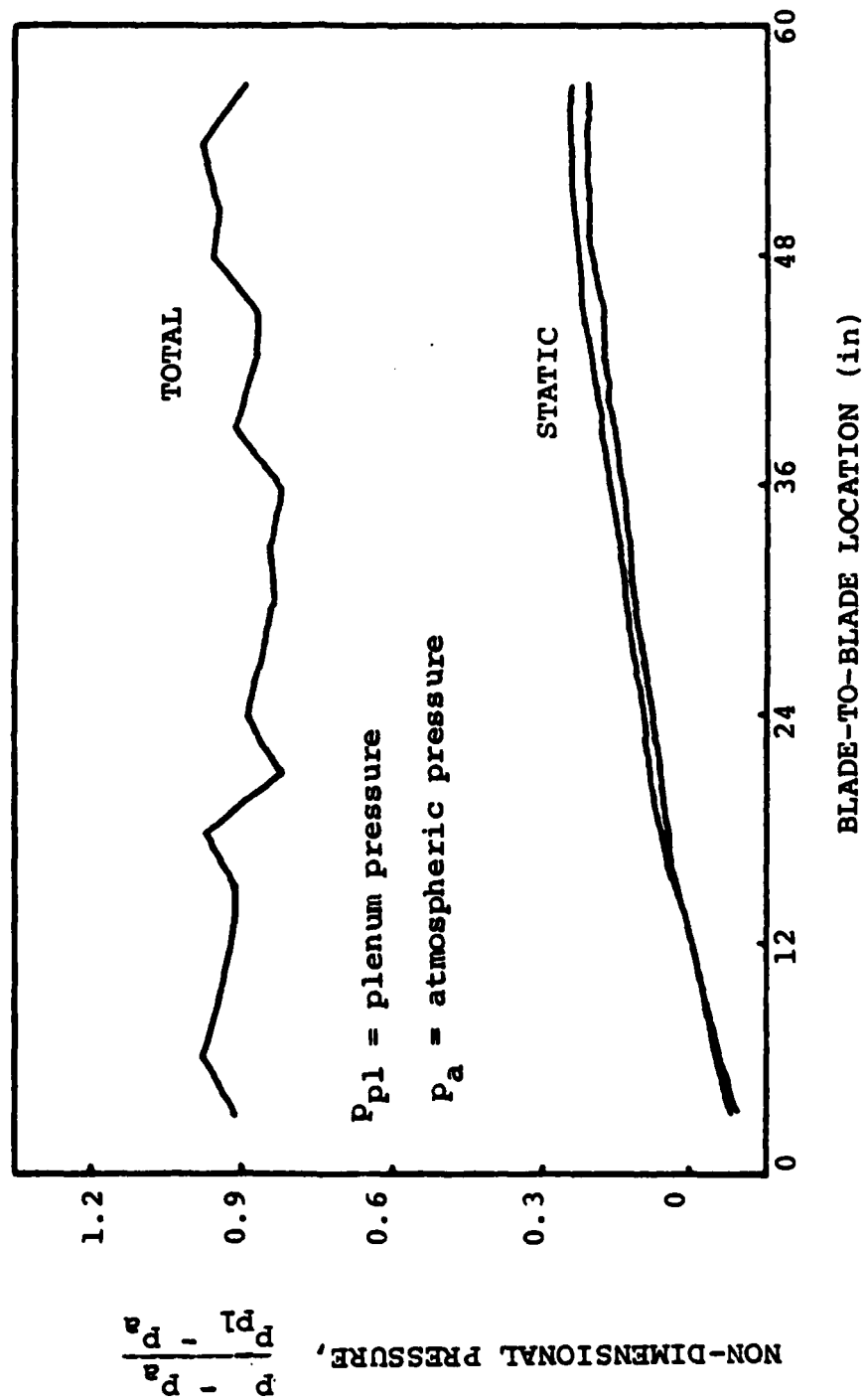
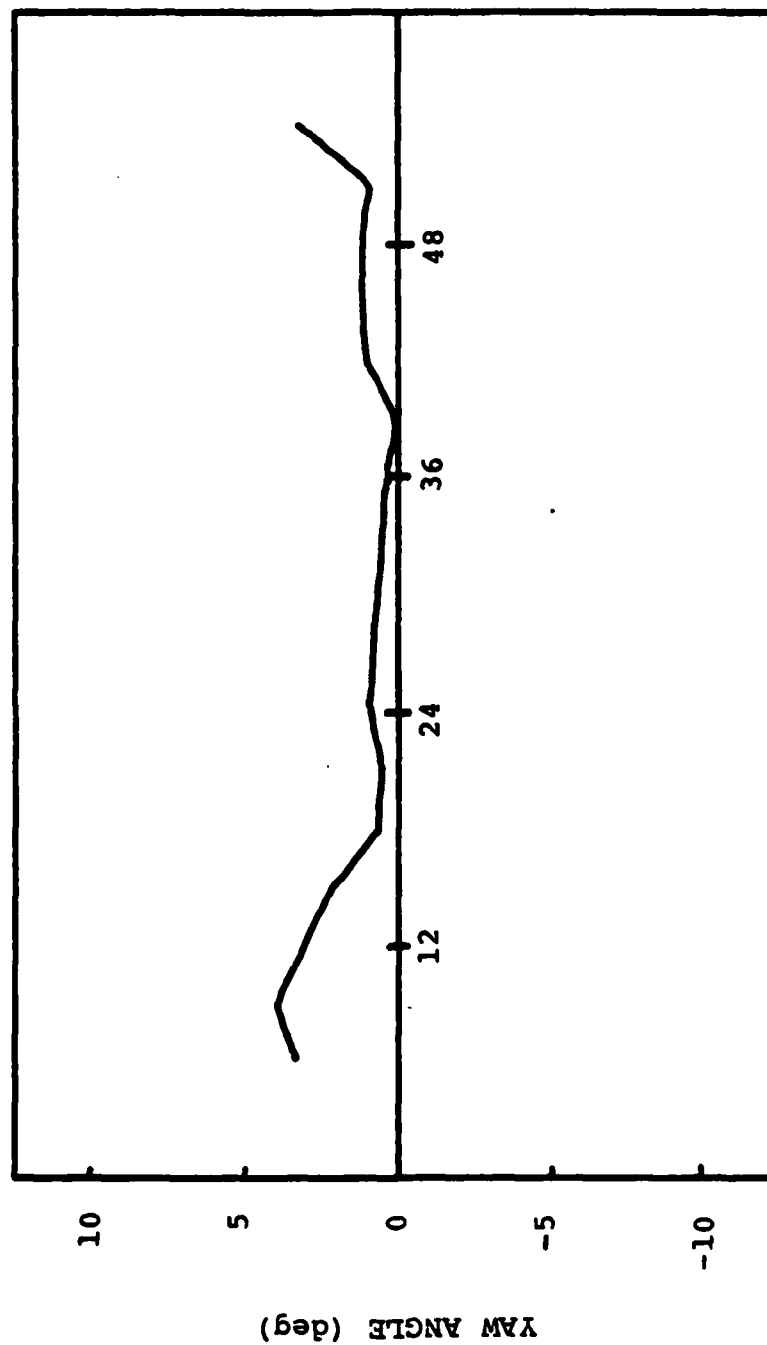


FIGURE A4. NON-DIMENSIONAL PRESSURE VS. BLADE-TO-BLADE LOCATION WITHOUT BAFFLES AND DIVERTER PLATE IN THE PLENUM. (3-inch intervals)



BLADE-TO-BLADE LOCATION (in)

FIGURE A5. YAW ANGLE DISTRIBUTION WITHOUT BAFFLES AND DIVERTER PLATE IN THE PLENUM.

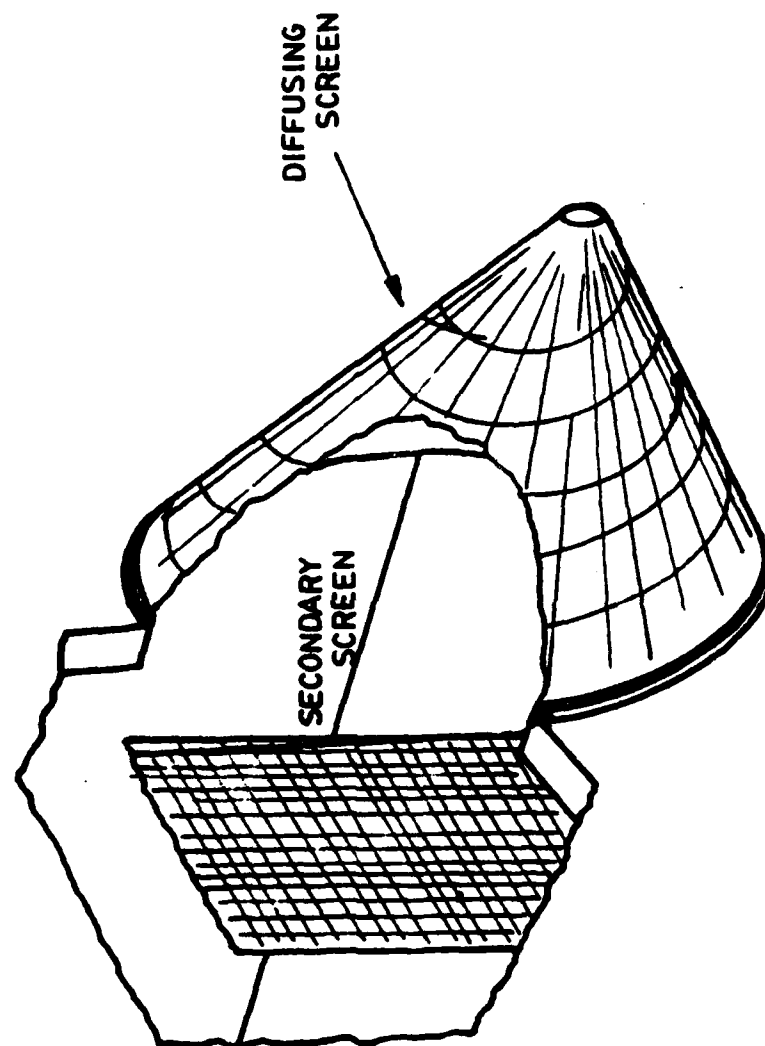


FIGURE A6. DIFFUSING SCREEN ARRANGEMENT ON BLOWER EXIT

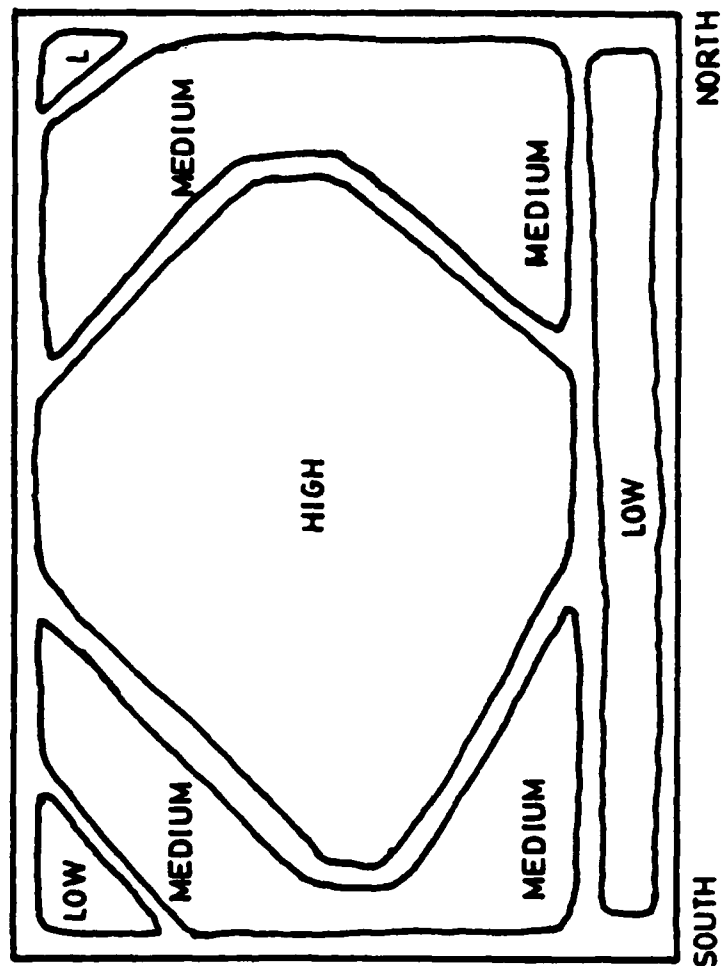


FIGURE A7. RELATIVE VELOCITIES EXITING SOUND BAFFLES WITH DIFFUSING SCREEN ARRANGEMENT ON BLOWER EXIT.

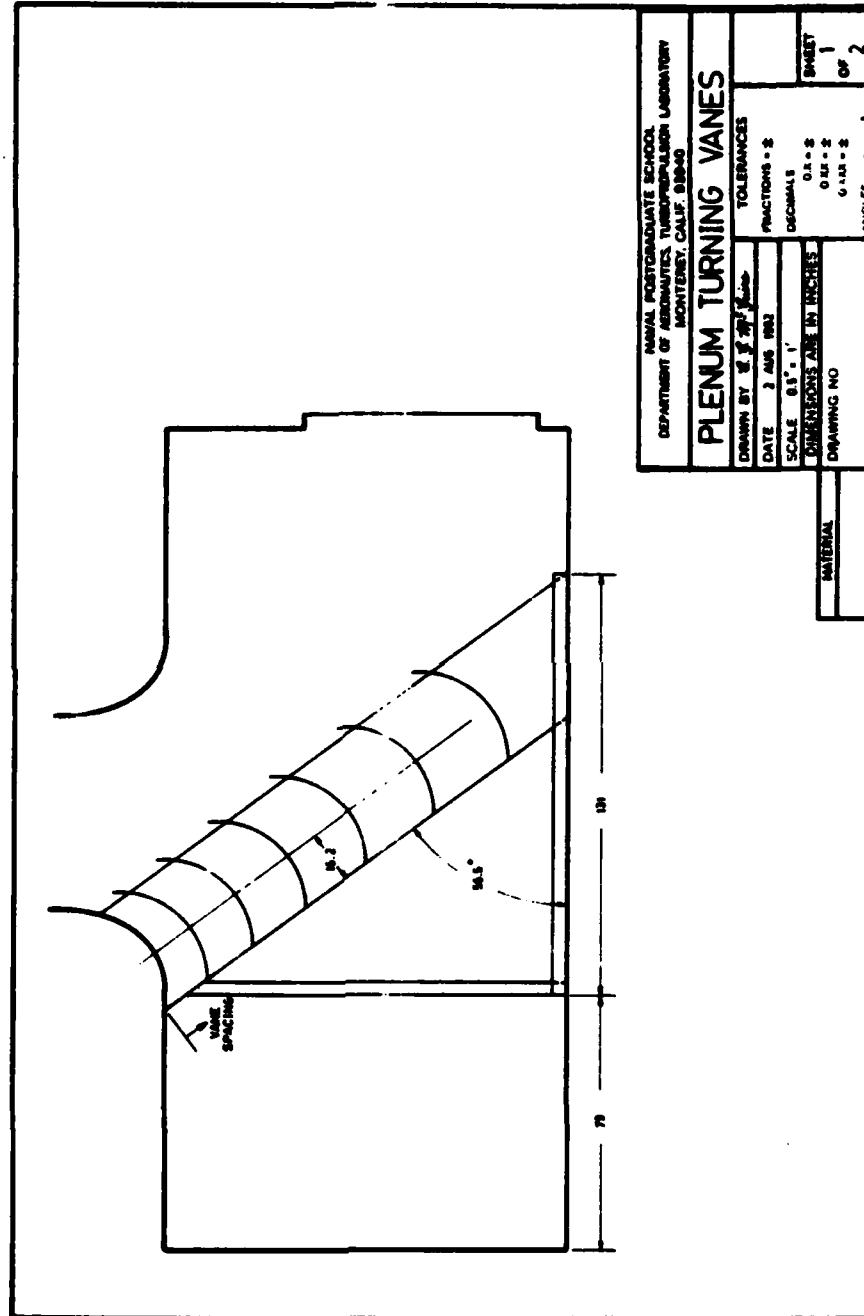
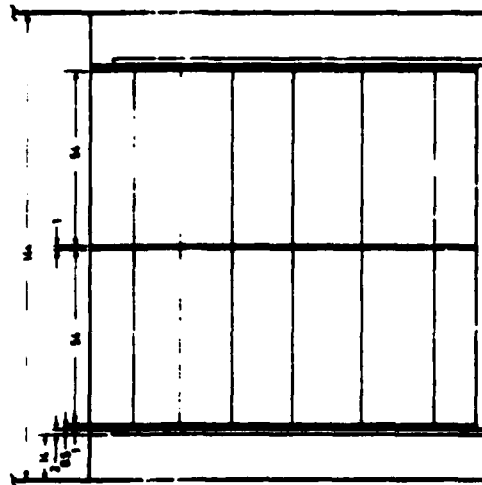


FIGURE A8a. PLENUM TURNING VANES, SIDE VIEW.



VANE TO VANE SPACING	
VANE	SPACING
1	16.30
2	17.00
3	18.40
4	21.10
5	25.50
6	27.0

VANE VANES MUST BEH 16" WITH A 27" BARRIS

NAVAL POSTGRADUATE SCHOOL
DEPARTMENT OF AERONAUTICS TURBOMACHINERY LABORATORY
MONTEREY, CALIF. 93940

PLENUM TURNING VANES

DRAWN BY <i>2/2/7</i>	TOLERANCES	
DATE 20 JUL 1960	FRACTIONS - 2	
SCALE 8" = 1'-0"	DECIMALS	
EXCEPTIONS ARE IN INCHES	0.1 - 2	
DRAWING NO	0.01 - 2	
	ANGLES	
		SHEET
		2
		(1)
		2

FIGURE A8b. PLENUM TURNING VANES, FRONT VIEW.

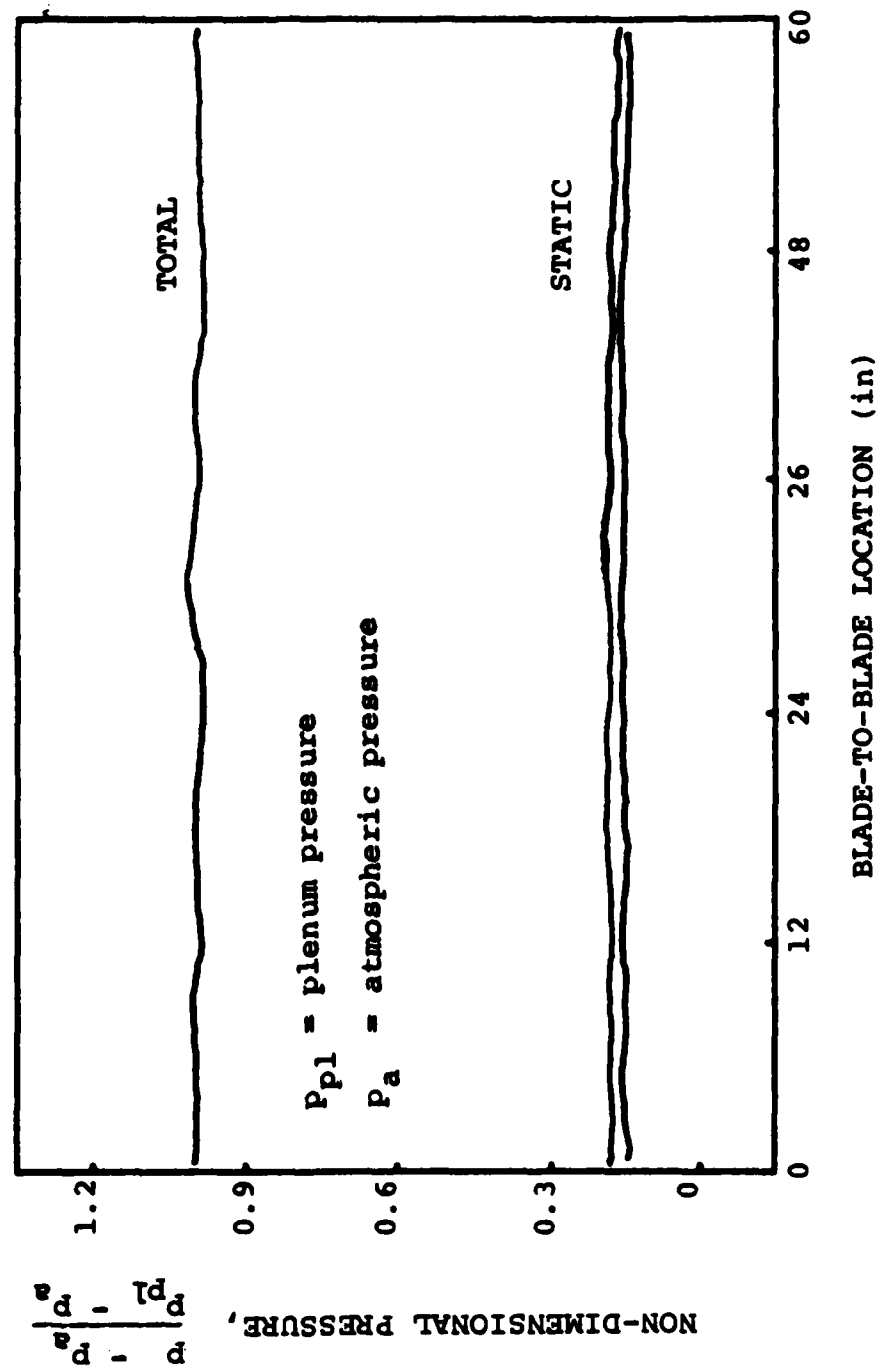


FIGURE A9. NON-DIMENSIONAL PRESSURE VERSUS BLADE-TO-BLADE LOCATION WITH TURNING VANES IN THE PLENUM. (3-inch intervals)

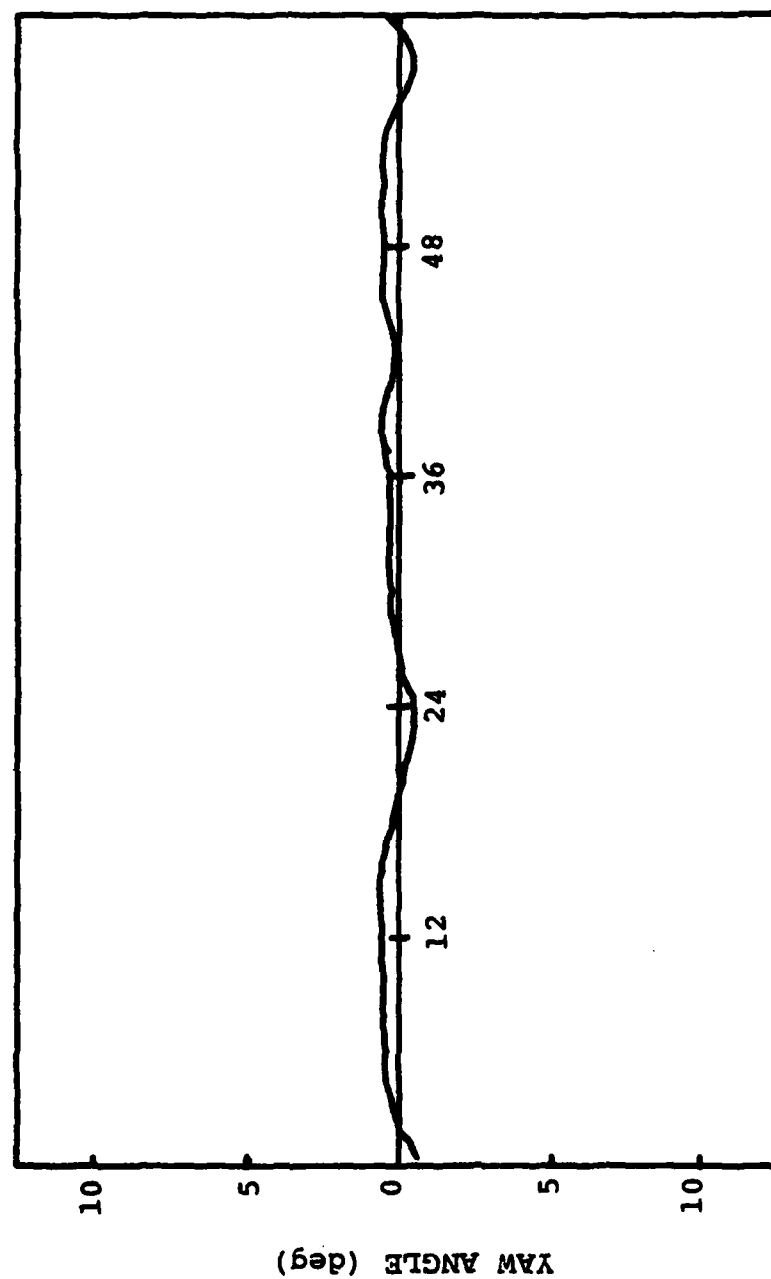


FIGURE A10. YAW ANGLE DISTRIBUTION WITH TURNING VANES IN THE PLENUM.

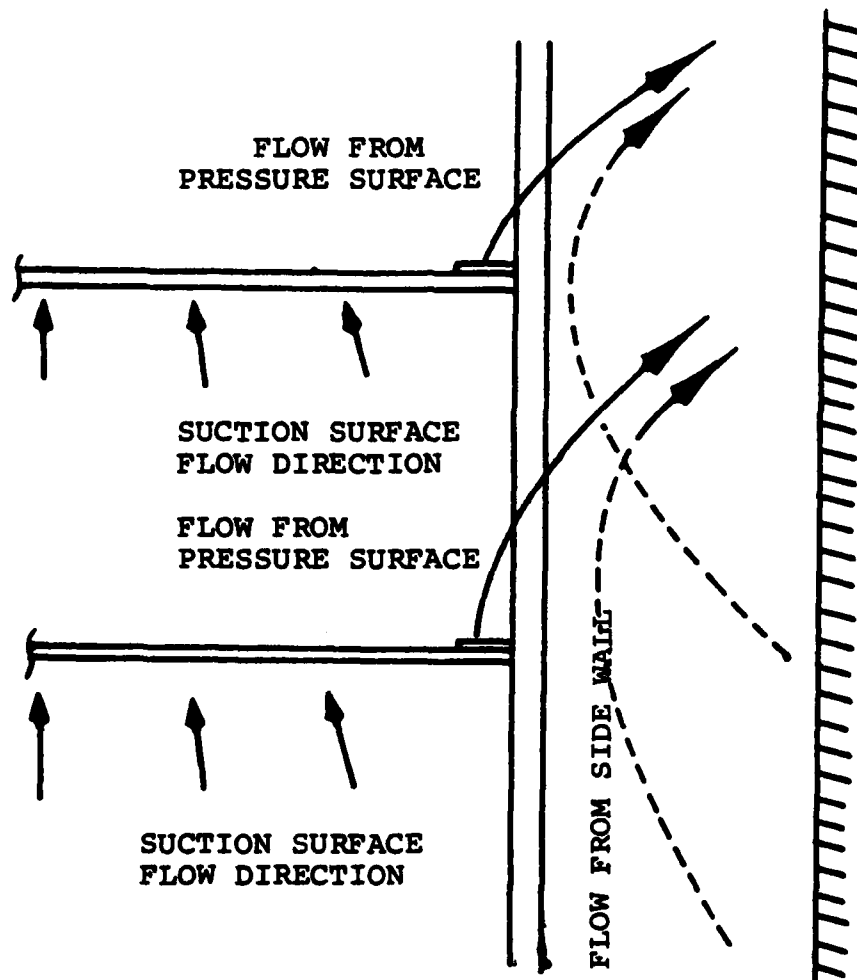


FIGURE A11. VORTEX FLOW AROUND ENDS OF TURNING VANES.

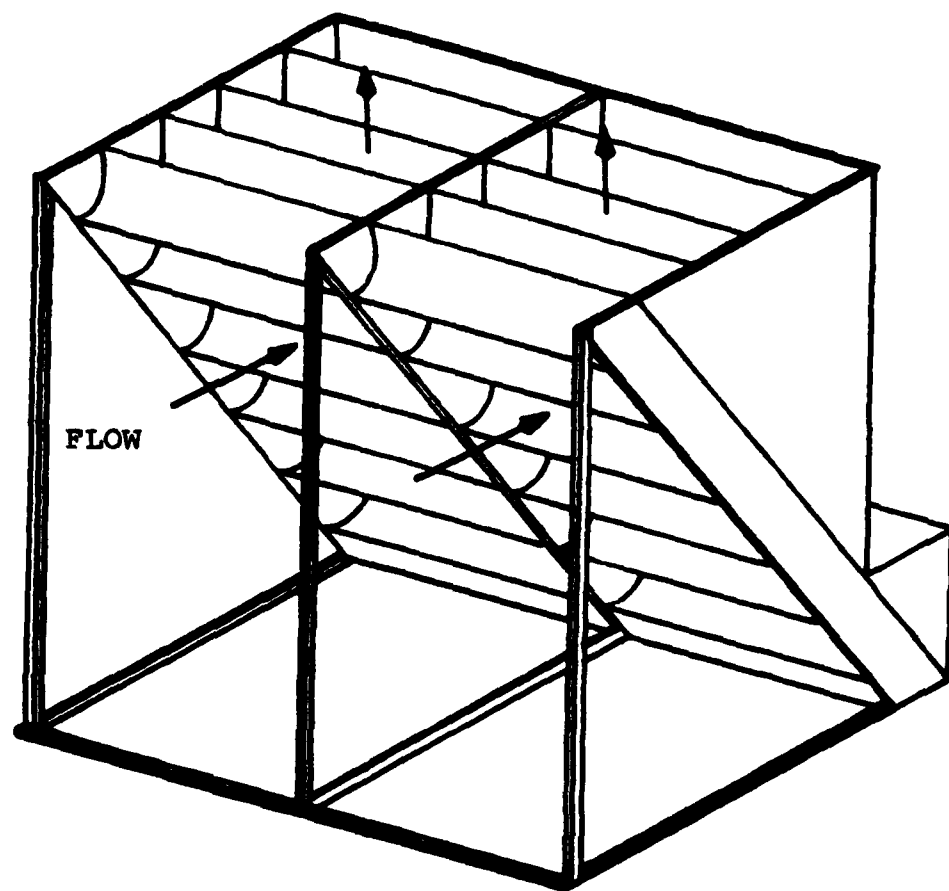


FIGURE A12. ENCLOSED TURNING VANE ARRAY.

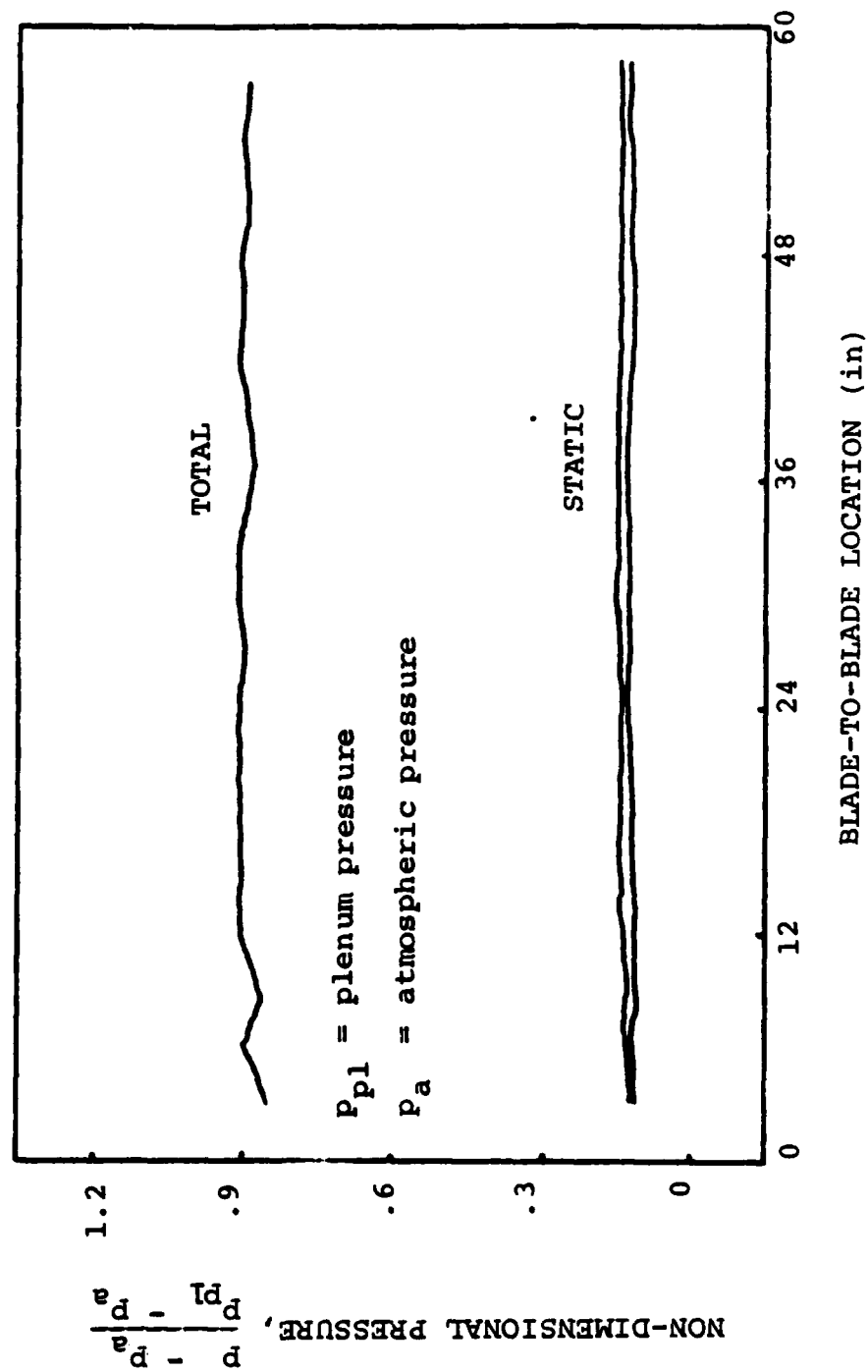
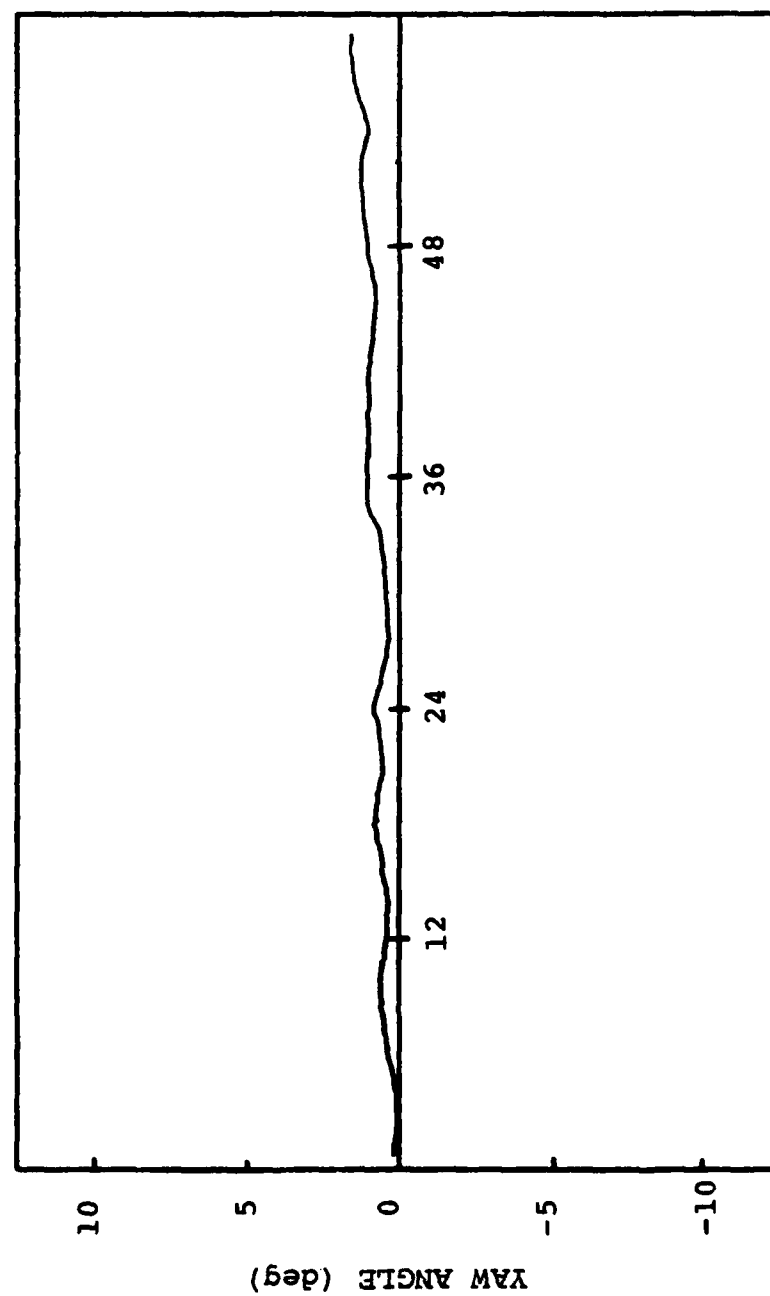


FIGURE A13. NON-DIMENSIONAL PRESSURE VS. BLADE-TO-BLADE LOCATION WITH ENCLOSED TURNING VANES. (3-inch intervals)



BLADE-TO-BLADE LOCATION (in)

FIGURE A14. YAW ANGLE DISTRIBUTION WITH ENCLOSED TURNING VANES.

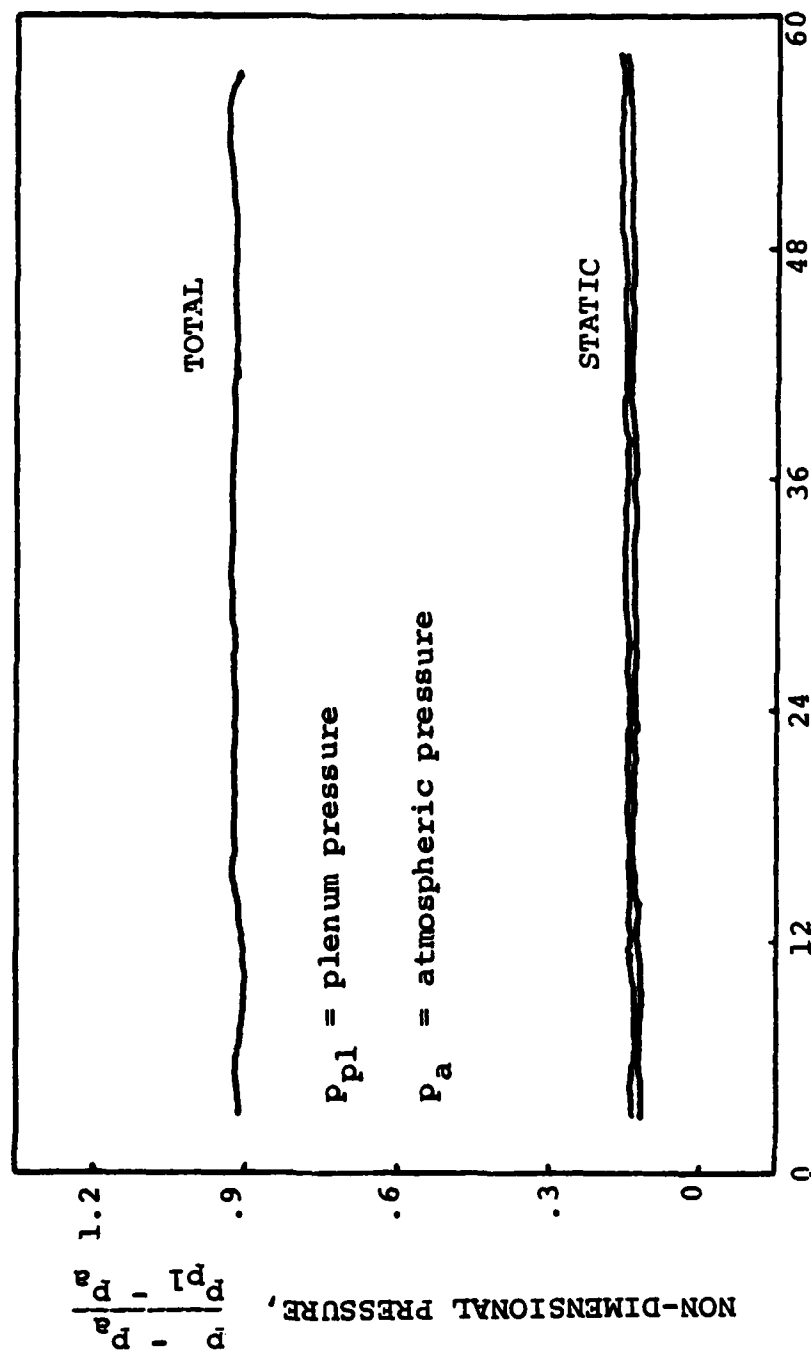


FIGURE A15. NON-DIMENSIONAL PRESSURE VS. BLADE-TO-BLADE LOCATION WITH ENCLOSED TURNING VANES AND $\beta_1 = 39.2^\circ$. (3-inch intervals)

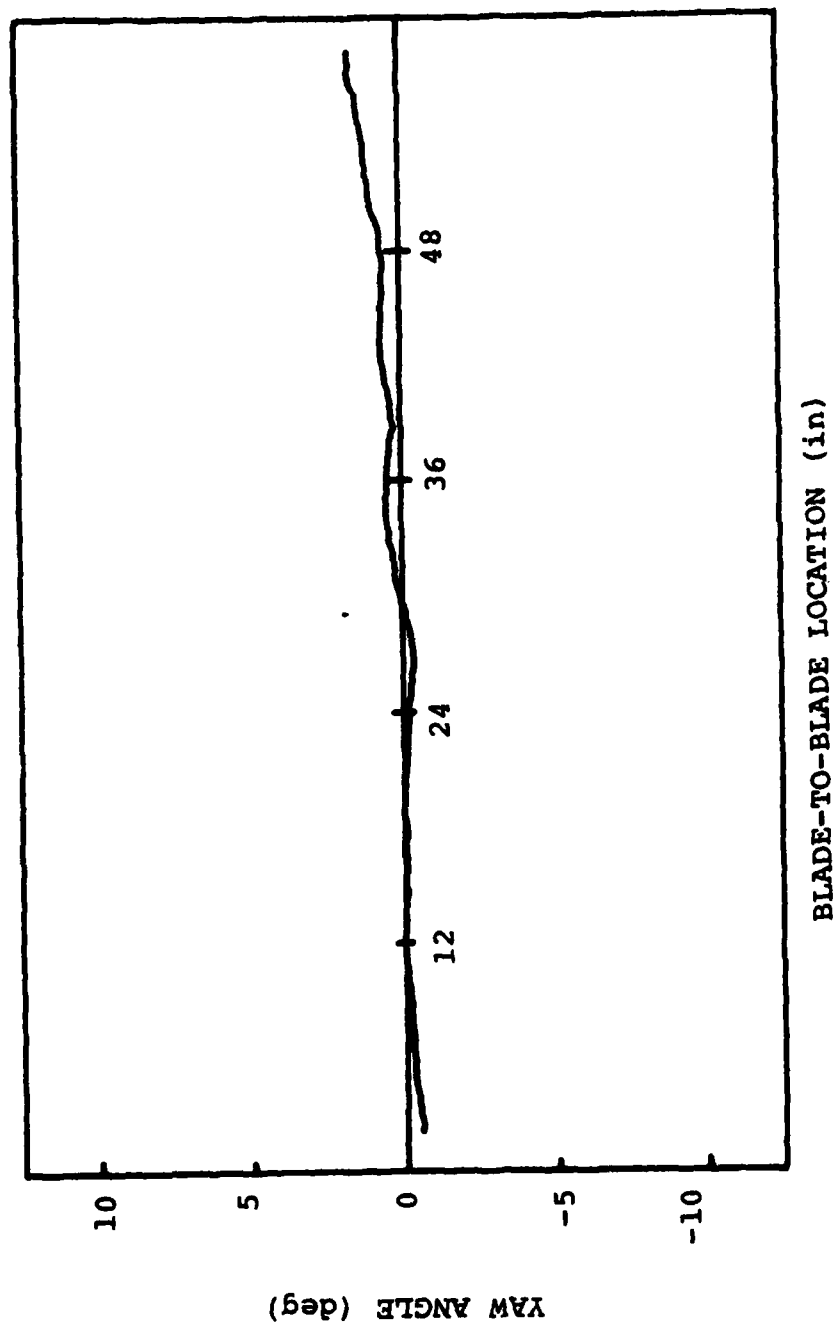


FIGURE A16. YAW ANGLE DISTRIBUTION WITH ENCLOSED TURNING VANES AND $\beta_1 = 39.2^\circ$.

LIST OF REFERENCES

1. Sanger, N. L., The Use of Optimization Techniques to Design Controlled Diffusion Compressor Blading, NASA TM 82763, 1982.
2. Rose, C. and Guttormson, D. L., Installation and Test of a Rectilinear Cascade, Master's Thesis, Naval Postgraduate School, Monterey, California, 1964.
3. Bartocci, J. E., An Investigation of the Flow Conditions at the Lower Measuring Plane and in the Plenum Chamber of the Rectilinear Cascade, Master's Thesis, Naval Postgraduate School, Monterey, California, 1966.
4. Moebius, R. C., Analysis and Testing to Improve the Flow from the Plenum of a Subsonic Cascade Wind Tunnel, Master's Thesis, Naval Postgraduate School, Monterey, California, 1980.
5. Himes, S. J., Report of Tests of a Compressor Configuration of DCA Blading, Master's Thesis, Naval Postgraduate School, Monterey, California, 1983.
6. Pankhurst, R. C. and Holder, D. W., Wind Tunnel Technique, An Account of Experimental Methods Used in Low and High Speed Wind Tunnels, Pitman and Sons, Ltd., 1952.
7. Todd, J. P. and Ellis, H. B., Applied Heat Transfer, Harper and Rowe, 1982.
8. Schlichting, H., Boundary Layer Theory, McGraw-Hill, 1979.
9. Cina, F. S., Subsonic Cascade Wind Tunnel Tests Using a Compressor Configuration of DCA Blades, Master's Thesis, Naval Postgraduate School, Monterey, California, 1981.
10. Molloy, W. D., Preliminary Measurements and Code Calculations of Flow Through a Cascade of DCA Blading at a Solidity of 1.67, Master's Thesis, Naval Postgraduate School, Monterey, California, 1982.
11. Idel'chik, I. E., Handbook of Hydraulic Resistance, Israel Program for Scientific Translations Ltd., 1966.

INITIAL DISTRIBUTION LIST

	No. Copies
1. Defense Technical Information Center Cameron Station Alexandria, VA 22314	2
2. Library, Code 0142 Naval Postgraduate School Monterey, CA 93943	2
3. Department Chairman, Code 67 Department of Aeronautics Naval Postgraduate School Monterey, CA 93943	1
4. Director Turbopropulsion Laboratory, Code 67Sf Department of Aeronautics Naval Postgraduate School Monterey, CA 93943	12
5. Mr. George Derderian Naval Air Systems Command Code AIR-310E Department of the Navy Washington, DC 20360	1
6. Dr. A. D. Wood Office of Naval Research Eastern/Central Regional Office 666 Summer Street Boston, MA 02210	1
7. Chief, Fan and Compressor Branch (Attn: Nelson Sanger) NASA Lewis Research Center Mail Stop 5-9 21000 Brookpark Road Cleveland, OH 44135	1
8. Mr. Alan G. McGuire 570 Ocean Avenue, #708 Monterey, CA 93940	2

END

FILMED

3-84

DTIC